

## 4 Nuclear Magnetic Resonance

Pieter Zeeman observed in 1896 the splitting of optical spectral lines in the field of an electromagnet. Since then, the splitting of energy levels proportional to an external magnetic field has been called the "Zeeman effect". The "Zeeman resonance effect" causes magnetic resonances which are classified under radio frequency spectroscopy (rf spectroscopy).

In these resonances, the transitions between two branches of a single energy level split in an external magnetic field are measured in the megahertz and gigahertz range. In 1944, Jevgeni Konstantinovitch Savoiski discovered electron paramagnetic resonance. Shortly thereafter in 1945, nuclear magnetic resonance was demonstrated almost simultaneously in Boston by Edward Mills Purcell and in Stanford by Felix Bloch. Nuclear magnetic resonance was sometimes called nuclear induction or paramagnetic nuclear resonance. It is generally abbreviated to NMR. So as not to scare prospective patients in medicine, reference to the "nuclear" character of NMR is dropped and the magnetic resonance based imaging systems (scanner) found in hospitals are simply referred to as "magnetic resonance imaging" (MRI).

### 4.1 The Nuclear Resonance Effect

Many atomic nuclei have spin, characterized by the nuclear spin quantum number  $I$ . The absolute value of the spin angular momentum is

$$|L| = \hbar \sqrt{I(I+1)}. \quad (4.01)$$

The component in the direction of an applied field is

$$L_z = I_z \hbar \equiv m \hbar. \quad (4.02)$$

The external field is usually defined along the  $z$ -direction. The magnetic quantum number is symbolized by  $I_z$  or  $m$  and can have  $2I+1$  values:

$$I_z \equiv m = -I, -I+1, \dots, I-1, I. \quad (4.03)$$

It holds for  $I$  that

- $I$  is half-integer for uneven mass numbers;
- $I$  is a whole number for even mass numbers but uneven proton numbers;
- $I$  is zero for even mass numbers and even numbers of protons.

The nucleus  $^1\text{H}$  is studied in the greatest number of NMR papers. In Current Contents<sup>®</sup> Physics, Chemistry, and Earth Sciences for the year 2000, approximately 9000 papers were published relating to NMR. 35% of these works refer to  $^1\text{H}$ , 25% to  $^{13}\text{C}$ , 8% to  $^{31}\text{P}$ , 8% to  $^{15}\text{N}$ , 4% to  $^{29}\text{Si}$  and 2% to  $^{19}\text{F}$  as the nucleus under study. In all these nuclei, the nuclear spin  $I = 1/2$ . If we look at nuclei with a quadruple moment and half-integer spin  $I > 1/2$ , we find the nucleus  $^{27}\text{Al}$  in 3% of all the NMR papers and 1% for each of the nuclei  $^{11}\text{B}$ ,  $^7\text{Li}$ ,  $^{23}\text{Na}$  and  $^{51}\text{V}$ . For even numbered spin, only the  $I = 1$  nuclei are frequently encountered:  $^2\text{H}$  in 4% and  $^{14}\text{N}$  and  $^6\text{Li}$  in 0,5% of all NMR papers.

Immeasurable Nuclei (those without nuclear spin), with even mass numbers and even proton numbers dominate the matter around us:  $^{16}_8\text{O}$ ,  $^{28}_{14}\text{Si}$  and  $^{12}_6\text{C}$ . To study such atoms using NMR, the sample is often enriched with isotopes of otherwise low natural abundance, for example  $^{13}_6\text{C}$  (natural abundance = 1%),  $^{29}_{14}\text{Si}$  (natural abundance = 5%) and  $^{17}_8\text{O}$  (natural abundance = 0.04%).

The magnetic moment of nuclei can be explained as follows: atomic nuclei carry electric charge. In nuclei with spin, the rotation creates a circular current which produces a magnetic moment  $\boldsymbol{\mu}$ . An external homogenous magnetic field  $\boldsymbol{B}$  results in a torque

$$\boldsymbol{T} = \boldsymbol{\mu} \times \boldsymbol{B} \quad (4.04)$$

with a related energy of

$$E = -\boldsymbol{\mu} \cdot \boldsymbol{B}. \quad (4.05)$$

Magnetic quantities are introduced in equ. (2.03). We will use the magnetic induction  $\boldsymbol{B}$  written in the units of Tesla ( $T = \text{Vs m}^{-2}$ ) to characterize the magnetic fields instead of the magnetic field strength  $\boldsymbol{H}$  in units of  $\text{A m}^{-1}$ . The magnetization  $\boldsymbol{M}$  corresponds to the sum of the magnetic dipole moments  $\boldsymbol{\mu}$  per unit volume.

The rotation of an electrically charged particle is termed gyration (Greek *Gyros* = circle). The gyromagnetic (actually magnetogyric) ratio  $\gamma$ , which is important for magnetic resonance, is defined by the equation

$$\boldsymbol{\mu} = \gamma \boldsymbol{L}. \quad (4.06)$$

The  $z$  component of the nuclear magnetic moment, cf. equ. (4.02), is

$$\mu_z = \gamma L_z = \gamma I_z \hbar \equiv \gamma m \hbar. \quad (4.07)$$

The energy level of a nucleus of nuclear spin  $I$  is thereby split in an external field in the  $z$ -direction  $\boldsymbol{B}_0$  into  $2I + 1$  Zeeman levels. The energy difference compared to the state without the magnetic field is

$$E_m = -\mu_z B_0 = -\gamma m \hbar B_0. \quad (4.08)$$

The macroscopic magnetization, which under the sole influence of an external field aligns itself in the same direction, is  $M_0 = \chi_0 H_0 = \chi_0 B_0 / \mu_0$ , see equ. (2.03). According to definition, it is equal to the sum of the  $N$  nuclear moments per unit volume. Using Boltzmann distribution with  $\exp(-E_m/kT) / \sum_m \exp(-E_m/kT)$ , we can calculate the occupation probability for the level  $m$ . From that it follows from the equations (4.07-08) and summation over all values of  $m$  that

$$M_0 = N \gamma \hbar \frac{\sum_{m=-I}^{m=+I} m \exp(\gamma \hbar m B_0 / kT)}{\sum_{m=-I}^{m=+I} \exp(\gamma \hbar m B_0 / kT)} = \frac{N \gamma^2 \hbar^2 I(I+1)}{3kT} B_0. \quad (4.09)$$

In the transition from the middle to the right hand side of equ. (4.09), the exponential function was expanded to the linear term. In the summation, use is made of  $\sum_m 1 = 2I + 1$ ,  $\sum_m m = 0$  and  $\sum_m m^2 = I(I+1)(2I+1)/3$ . Because  $M_0 = \chi_0 H_0 = \chi_0 B_0 / \mu_0$ , the quotient multiplied by  $\mu_0$  on the right hand side of equ. (4.09) represents the statistical nuclear susceptibility. It obeys the Currier law  $\chi_0 = C/T$ , in which the Currier constant  $C$  is found using equ. (4.09).

When  $I = 1/2$ ,  $m = \pm 1/2$ , we get two levels with an energy difference of

$$\Delta E_{-1/2,+1/2} = \gamma \hbar B_0 = \hbar \omega_L = h \nu_L. \quad (4.10)$$

In equ. (4.10) the energy difference has been replaced by the resonant frequency, which is named after Joseph Larmor, who in 1897 described the precession of orbital magnetization in an external magnetic field. The Larmor frequency  $\nu_L$  (or Larmor angular frequency  $\omega_L$ ) can be described using a classical model: the torque  $\mathbf{T}$  acting on a magnetic dipole is defined as the time derivative of the angular momentum  $\mathbf{L}$ . For this reason, in consideration of equ. (4.06), we get

$$\mathbf{T} = \frac{d\mathbf{L}}{dt} = \frac{1}{\gamma} \frac{d\boldsymbol{\mu}}{dt}. \quad (4.11)$$

By setting this equal to equ. (4.04),  $\mathbf{T} = \boldsymbol{\mu} \times \mathbf{B}$ , we see that

$$\frac{d\boldsymbol{\mu}}{dt} = \gamma \boldsymbol{\mu} \times \mathbf{B}. \quad (4.12)$$

The summation of all nuclear dipoles in the unit volume gives us the magnetization. For a magnetization that has not aligned itself parallel to the external magnetic field, it is necessary to solve the following equation of motion

$$\frac{d\mathbf{M}}{dt} = \gamma \mathbf{M} \times \mathbf{B}. \quad (4.13)$$

It is usual to define  $\mathbf{B} = (0, 0, B_0)$ . If we choose  $\mathbf{M}(t=0) = |\mathbf{M}| (\sin\alpha, 0, \cos\alpha)$  as initial conditions, the solutions are

$$\begin{aligned} M_x &= |\mathbf{M}| \sin\alpha \cos\omega_L t, \\ M_y &= |\mathbf{M}| \sin\alpha \sin\omega_L t, \\ M_z &= |\mathbf{M}| \cos\alpha, \end{aligned} \quad (4.14)$$

in which  $\omega_L = -\gamma B_0$  has been used. If the rotation is described by a vector in the direction of the axis of rotation, we have

$$\boldsymbol{\omega}_L = -\gamma \mathbf{B}_0. \quad (4.15)$$

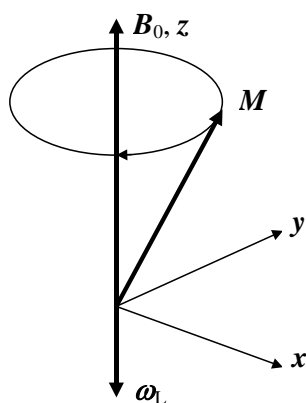


**Fig. 4.1** Larmor precession around the external magnetic field.

The rotation vector is thus opposed to  $\mathbf{B}_0$  for positive values of  $\gamma$ . For negative values of  $\gamma$ , both directions are the same. The Larmor relationship is most commonly given as an equation of magnitudes in the form  $\omega_L = \gamma B_0$  or

$$\nu_L = \frac{\gamma}{2\pi} B_0. \quad (4.16)$$

This most important equation of NMR relates the magnetic field to the resonant frequency.

A few values for  $\gamma/2\pi$  are given in Tab. 4.1. With iron-core and superconductive magnets, modern NMR magnets of 2,4 and 24 Tesla can be built; with those we would get nuclear magnetic resonance frequencies for  $^1\text{H}$  nuclei of 100 and 1000 MHz, respectively.

**Table 4.1** Gyromagnetic ratio  $\gamma/2\pi$  in units of MHz/T, nuclear spin and natural abundance of a few nuclei. To get the Larmor frequency  $\nu_L$  from  $\gamma/2\pi$ , we have to multiply with the corresponding value of magnetic induction. A few common values are ( $\nu_L$  for  $^1\text{H}$  is written in parentheses): 2,3488 T (100 MHz), 7,0463 T (300 MHz), 11,7440 T (500 MHz), 17,6157 T (750 MHz), 21,1389 T (900 MHz).

$^1\text{H}$	42,58	1/2	99,98%	$^{19}\text{F}$	40,05	1/2	100%	$^{63}\text{Cu}$	11,28	3/2	69,99%	$^{121}\text{Sb}$	10,19	5/2	57,25%
$^2\text{H}$	6,535	1	0,015%	$^{23}\text{Na}$	11,42	3/2	100%	$^{65}\text{Cu}$	12,09	3/2	30,91%	$^{127}\text{I}$	8,518	5/2	100%
$^7\text{Li}$	16,55	3/2	92,58%	$^{27}\text{Al}$	11,09	5/2	100%	$^{75}\text{As}$	7,291	3/2	100%	$^{133}\text{Cs}$	5,584	7/2	100%
$^9\text{Be}$	5,984	3/2	100%	$^{29}\text{Si}$	8,458	1/2	4,7%	$^{77}\text{Se}$	8,118	1/2	7,58%	$^{195}\text{Pt}$	9,153	1/2	33,8%
$^{10}\text{B}$	4,575	3	19,58%	$^{31}\text{P}$	17,24	1/2	100%	$^{79}\text{Br}$	10,67	3/2	50,54%	$^{199}\text{Hg}$	7,590	1/2	16,84%
$^{11}\text{B}$	13,66	3/2	80,42%	$^{35}\text{Cl}$	4,172	3/2	75,53%	$^{81}\text{Br}$	11,50	3/2	49,46%	$^{201}\text{Hg}$	2,809	3/2	13,22%
$^{13}\text{C}$	10,71	1/2	1,108%	$^{37}\text{Cl}$	3,473	3/2	24,47%	$^{87}\text{Rb}$	13,93	3/2	27,85%	$^{203}\text{Tl}$	24,33	1/2	29,5%
$^{14}\text{N}$	3,076	1	99,63%	$^{51}\text{V}$	11,19	7/2	99,76%	$^{93}\text{Nb}$	10,41	9/2	100%	$^{205}\text{Tl}$	24,57	1/2	70,5%
$^{15}\text{N}$	4,314	1/2	0,37%	$^{55}\text{Mn}$	10,50	5/2	100%	$^{117}\text{Sn}$	15,17	1/2	7,61%	$^{207}\text{Pb}$	8,907	1/2	22,6%
$^{17}\text{O}$	5,772	5/2	$3,7 \cdot 10^{-2}$	$^{59}\text{Co}$	10,05	7/2	100%	$^{119}\text{Sn}$	15,87	1/2	8,58%	$^{209}\text{Bi}$	6,841	9/2	100%

At the end of the introduction, the difference between the nuclear magnetic resonance and the actual nuclear resonance will be presented. The  $^{57}_{26}\text{Fe}$  isotope in an external magnetic field is often observed in the recoil free  $\gamma$ -radiation resonant absorption (Mössbauer effect, see chapter 9). In this case, there are transitions between the nuclear ground state and an excited nuclear level 14,4 keV higher with a half-life of around  $10^{-7}$  s. This state is occupied by the capture of an electron in the K shell by the nucleus  $^{57}_{27}\text{Co}$  (half-life: 270 days). In the ground state, the nucleus has spin  $I = 1/2$  and gyromagnetic ratio  $\gamma/2\pi = 1,38$  MHz/T. In the excited state we are considering, the nucleus has spin  $I = 3/2$  and a negative gyromagnetic ratio  $\gamma/2\pi = -2,39$  MHz/T. A representation of Zeeman splitting (not to scale) is shown in Fig. 4.2. The energy difference of the two nuclear levels is  $E_a - E_g = 14,4$  keV, expressed as a frequency:  $3,5 \times 10^{18}$  Hz. The Zeeman splitting of the Mössbauer spectrum into six lines in a field of 1 Tesla is about 12 orders of magnitude smaller. The NMR transition is only observable for ground states due to detector sensitivity.

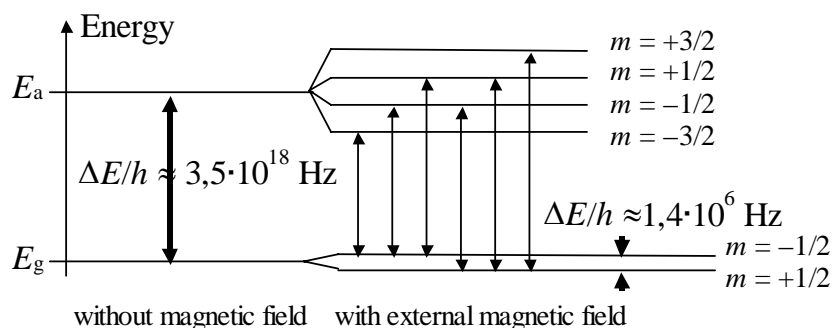


**Fig. 4.2.** Zeeman splitting of the nuclear levels for the Mössbauer transition in  $^{57}_{26}\text{Fe}$ -nuclei.

## 4.2 Basic Set-up of NMR Spectrometers

A greatly simplified construction plan for an NMR spectrometer is shown in Fig. 4.3. A high frequency generator drives a transmitter either continuously (*cw*-spectrometers, see below) or with an electronic switch (pulse spectrometer). The high frequency creates a high frequency field in a coil surrounding the sample. This coil/sample arrangement is submersed in the static magnetic field of a generally superconducting magnet. The receiver measures the absorption (*cw*-spectrometer) or free induction decay in the coil (pulse spectrometer). After analog-to-digital conversion, a computer takes over further signal processing.

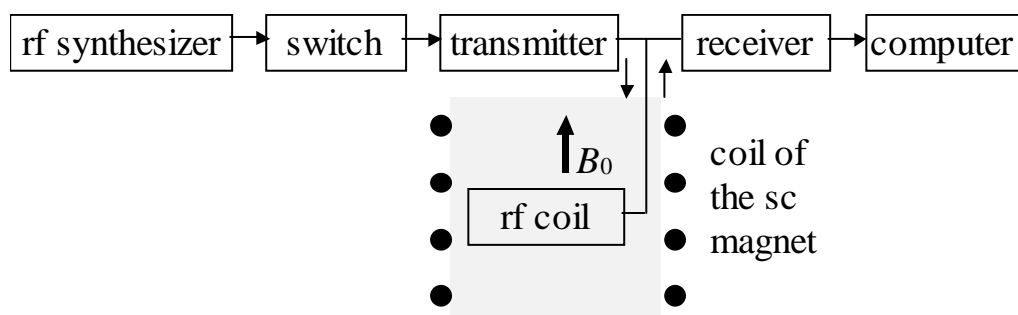


**Fig. 4.3** Basic set-up of an NMR spectrometer.

*Continuous wave spectrometers with stationary rf input* are rarely applied these days. To prevent saturation effects, they use a weak rf input of a few  $\mu\text{T}$  at constant frequency with variable magnetic field or vice-versa. For broad lines, the line is scanned differentially in a way similar to that used in ESR (see chapter 5). The absorption signal (or its derivative in the case of differential scanning) is obtained directly as a function of the field or frequency, as shown in Fig. 4.4.

*Pulse spectrometers* input high frequency pulses. In the study of liquids, rf induction in the mT range is sufficient, whereas in the study of solids, maximal rf induction and minimal pulse width is desired, for example: 12 mT with an pulse length  $\tau_{\pi/2}$  of 1  $\mu\text{s}$  is necessary to rotate the magnetization of  $^1\text{H}$ -nuclei from the  $z$ -direction into the  $x$ - $y$ -plane. The nutation of the magnetization through the angle  $\pi/2$  ( $\pi/2$ -pulse means  $\gamma B_{\text{rf}} \tau_{\pi/2} = \pi/2$ ) is described in equ. (4.13), if we set  $\mathbf{B} = (B_{\text{rf}} \cos \omega t, 0, B_0)$ .

*Pulse spectrometers* work at a constant frequency and constant magnetic field. The signal is obtained by the free induction decay (FID) when the pulse is switched off. Due to ring down effect of the pulse in the rf coil and other electronic effects connected to the strength of the transmitter pulse at the input stage of the amplifier, we get a ring down delay and a receiver dead-time of a few microseconds which unfortunately makes the observation of quickly decaying signals difficult. If it is possible to produce spin-echo, the delay in the reception of the signal is unimportant. Pulse spectrometers use phase sensitive rectification of the nuclear induction with the transmitter frequency. The signal is therefore the nuclear induction in the time domain modulated with the phase difference between the nuclear induction and transmitter frequency

The FID shown in Fig. 4.4 is not very useful for visual analysis. The usual spectrum in the frequency domain is found after the Fourier transformation of the signal which was measured as a function of time. The Fourier transform was introduced in equ. (2.67). An NMR spectrum is not, however, usually shown as a function of frequency  $\nu$  but rather on a scale of the chemical displacement  $\delta = (\nu_{\text{ref}} - \nu) / \nu_L$ , which we will explain in chapter 4.4. Such a spectrum is shown in Fig. 4.4. The inverse Fourier transformation of equ. (2.66) takes the frequency spectrum back to the time-dependent signal of the free induction. It corresponds to the transformation from Fig. 4.4 on the right into Fig. 4.4 on the left.

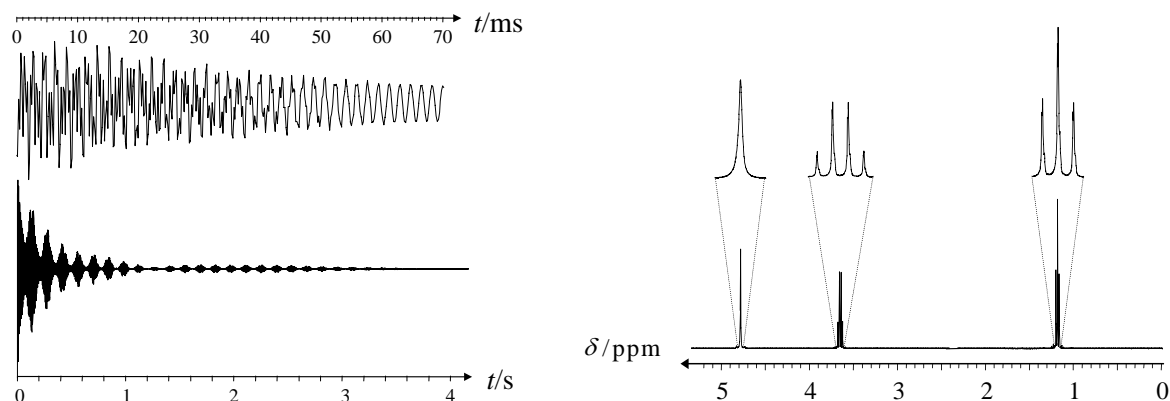


**Fig. 4.4** The free induction decay (FID, measured at a Larmor frequency of 400 MHz) as a function of time and the Fourier transformed  $^1\text{H}$  NMR spectrum of alcohol in fully deuterated water (courtesy of Dr. M. Findeisen; Leipzig). In the spectrum, the individual spikes above are expanded by a factor of 10. One ppm corresponds here to 400 Hz. The singlet comes from the OH groups, which exchange with the hydrogen nuclei of the solvent and therefore show no splitting. The quartet is caused by the  $\text{CH}_2$  groups, and the triplet corresponds to the  $\text{CH}_3$  group of the ethanol as will be explained in chapter 4.5

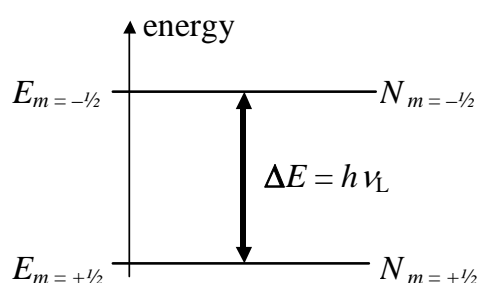
The spectrum displayed in Fig. 4.4 was taken at  $\nu_L = 400$  MHz and has lines separated by about 8 Hz. That corresponds to  $2 \cdot 10^{-8}$  times the Larmor frequency. For this resolution, homogeneity better than  $10^{-8}$  in the sample area is required, as is a magnetic field equally stable in time. By varying the currents in multiple shim coils in the vicinity of the sample head, the homogeneity of the static magnetic field can be improved. In the first iron magnets, homogenization was achieved by changing the geometry of the iron core. This is where the term "shim" originates. Improvement of the homogeneity in a plane can be achieved by rotating the sample around an axis perpendicular to it. The frequency of rotation has to be greater than the frequency dependencies caused by the inhomogeneities in the plane. Common values lie in the range of 10 Hz.

The first NMR pulse spectrometers used for high resolution of the signals of liquid substances were called Fourier spectrometers, since it is necessary to use a Fourier transformation to get a frequency spectrum from the free induction. The use of the Fourier technique brought, along with many other advantages, a clear increase in sensitivity compared to the *cw* technique. If we take another look at Fig. 4.4, the spectrum covers a frequency range of about 5 ppm or 2000 Hz. If we leave out the part of the spectrum in which the signal is zero, only about 100 Hz remain as the sum of the spectral widths of the signals. Using the *cw* technique, the entire range of the spectrum is scanned regardless of whether an absorption is observed. The Fourier technique excites the spins in the entire spectral range at the same time and observes them simultaneously. The measuring of the spectrum in Fig. 4.4 is therefore associated with an increase in sensitivity of  $2000 \text{ Hz} / 100 \text{ Hz} = 20$ . We will encounter similar situations in Fourier IR spectroscopy (chapter 7) and Fourier mass spectrometry (chapter 10).

### 4.3 Nuclear Magnetic Relaxation Time and Measurement Sensitivity

Spectra are represented as functions of frequency or frequency shift. In contrast, relaxation times describe the time dependency of the generation or decay of certain orders. Many relaxation times are difficult or impossible to measure with *cw* Spectrometers. We will, however, show that in transversal relaxation, the relaxation time determined by the free induction decay is related to the line width of the frequency spectrum.

The study of nuclear magnetic relaxation has achieved certain independence in the study of dynamic processes, so that it is sometimes separated from the study of nuclear magnetic resonance. Nuclear magnetic relaxation is related to nuclear resonance, but it cannot be portrayed in a single nuclear resonance spectrum. Instead of one spectrum, the dependency of a relaxation time on the measurement frequency or observation temperature is plotted. The fundamental relaxation time of NMR is the longitudinal relaxation time  $T_1$  that will be explained now.



Consider the two levels  $m = -1/2$  and  $m = +1/2$  in Fig. 4.5. With Nuclear spin  $I = 1/2$  (e.g.  $^1\text{H}$ ,  $^{13}\text{C}$ ,  $^{15}\text{N}$ ,  $^{19}\text{F}$ ,  $^{29}\text{Si}$ ,  $^{31}\text{P}$ ), the only possible resonance transition occurs between the two Zeeman levels. For half-integer spin  $I > 1/2$ , this corresponds to the central transition since in further splitting of the lines caused by quadrupole interaction, the resonance of the central transition remains constant to the first order.

**Fig. 4.5** The transition  $m = +1/2 \leftrightarrow m = -1/2$ .

$h\nu_L \ll kT$  applies at least for temperatures above 1 K and for the Larmor frequencies below 1 GHz. Thus, spontaneous transitions can be neglected, and the probabilities for absorption and induced emission are equal. From chapter 2.4 it follows

$$P = B_{+1/2,-1/2} w_L = B_{-1/2,+1/2} w_L. \quad (4.17)$$

$B$  refers to the Einstein coefficients for induced transitions and  $w_L$  is the spectral radiation density at the Larmor Frequency. A measurable absorption (or emission) only occurs if there is a difference in the two occupation numbers  $N$ . In thermal equilibrium, the Boltzmann distribution applies to  $N$  and we have

$$\frac{N_{+1/2}}{N_{-1/2}} = \exp\left(\frac{\hbar\gamma B_0}{kT}\right) = \exp\left(\frac{h\nu_L}{kT}\right). \quad (4.18)$$

If  $\nu_L = 500$  MHz and  $T = 300$  K,  $h\nu_L/kT \approx 8 \times 10^{-5}$  is very small, and the exponential function in equ. (4.18) can, in a good approximation, be expanded to the linear term. From that we get

$$\frac{N_{+1/2} - N_{-1/2}}{N_{-1/2}} = \frac{n}{N_{-1/2}} \approx \frac{h\nu_L}{kT} \approx 8 \cdot 10^{-5}, \quad (4.19)$$

where  $n$  is the difference in the occupation numbers. The difference in the occupation numbers is thus very small, and can be quickly rebalanced by absorption under the influence of a continuously input rf field of the corresponding frequency. We then speak of total saturation of the transition, in which there is no further macroscopic magnetization.

On the other hand, since we see that in equ. (4.18) that as the temperature tends toward infinity, the difference between the occupation numbers tends to zero, we can use the difference in the occupation numbers to define a spin temperature. This "temperature" is not necessarily the same as the surrounding temperature. An inversion of the occupation numbers corresponds to a change of sign of the temperature, and the balancing of the occupation numbers leads to an infinite temperature of the spin system. All degrees of freedom of the system except for the spin (e.g. nuclear oscillations, rotations, translations, external fields) are called the lattice. Setting thermal equilibrium with this lattice can be done only through induced emission. The fluctuating fields in the material always have a finite frequency component at the Larmor frequency (though possibly extremely small), so that energy from the spin system can be passed to the lattice. The time development of the setting of equilibrium can be described after either switching off or on the external field  $B_0$  at time  $t = 0$  (difficult to do in practice) with

$$n = n_0 e^{\frac{-t}{T_1}} \quad \text{or} \quad n = n_0 \left( 1 - e^{\frac{-t}{T_1}} \right), \quad (4.20)$$

respectively.  $T_1$  is the longitudinal or spin-lattice relaxation time and  $n_0$  denotes the difference in the occupation numbers in the thermal equilibrium, if the external field is on. *Longitudinal relaxation time* because the magnetization orients itself parallel to the external magnetic field corresponding to the difference in the occupation of the two levels. The relation between the longitudinal relaxation time  $T_1$  and the transition probability  $P$  in a two level system is

$$1/T_1 = 2P = 2B_{-1/2,+1/2} w_L, \quad (4.21)$$

which follows from

$$\frac{dN_{+1/2}}{dt} = -P(N_{+1/2} - N_{-1/2}) = -Pn = -\frac{1}{2} \frac{n}{T_1} = \frac{1}{2} \frac{dn}{dt}, \quad (4.22)$$

where we used  $N_{+1/2} = 1/2 \{ (N_{+1/2} + N_{-1/2}) + n \}$  and  $dn/dt = -n/T_1$  from equ. (4.20). The difference in the occupation numbers  $n$  is proportional to  $B_0$  and depends on the temperature  $T$  in accordance with equations (4.18-19). The dependency of  $T_1$  on the value of the spectral density function at the resonant frequency  $\omega_L$  has to be discussed in detail for special interactions, as will be done below for a homo-nuclear two spin system.

In the introduction of equ. (4.20), we assumed at the right an activation of the external field at time  $t = 0$ . In practice, the value of  $T_1$  in the simplest case is measured with the aid of two pulses. In chapter 4.2 we described the  $\pi/2$ -pulse, which rotates a macroscopic magnetization in thermal equilibrium oriented parallel to the external magnetic field ( $z$ -direction) into the  $x$ - $y$ -plane. After the  $\pi/2$ - pulse there is no further magnetization in the  $z$ -direction, which, in the picture above (Fig. 4.5), corresponds to the disappearance of the difference in occupation numbers. Instead of a difference in population, which cannot be directly observed by NMR methods, we have an observable "coherence". The term "coherence" is used because the phases of all rotating nuclear spins are the same as the phase of the incoming high frequency through the strong high frequency field. With that, after the pulse, the rotation of the macroscopic magnetization into the  $x$ - $y$ -plane can be observed in the signal induced in the coil. This free induction (FID) or phase coherence of the spin decays with the transversal relaxation time  $T_2$ , which is yet to be discussed.

We will now consider the action of a  $\pi$  pulse, which has twice the length of a  $\pi/2$  pulse, i.e. for a pulse length  $\tau_\pi$ , it holds that  $\gamma B_{1f} \tau_\pi = \pi$ . An pulse of this type rotates the magnetization from the  $z$ -direction to its opposite, the  $-z$ -direction. In our picture, this corresponds to an inversion of the occupation numbers. If we consider the equations (4.18-19), this inversion of the populations can be described by a reversal of the sign of the temperature. Through the action of the  $\pi$  pulse, we create an equally large but "negative" temperature of the spin system. In this physically questionable though very useful "temperature" picture, the Boltzmann equation for thermal equilibrium is applied to a state not in thermal equilibrium.

With the  $\pi$  pulse, the population differences which are non-observable with NMR are reversed. Since no observable coherences are created, we still need a further  $\pi/2$  pulse to measure the  $T_1$ -relaxation after the  $\pi$  pulse (adjustment of the temperature of the spin system to the positive temperature of the lattice). This pulse has the already mentioned property that the population differences are converted into observable coherences. Taking phase relationships into consideration, the application of a  $\pi/2$  pulse directly after a  $\pi$  pulse results in a negative signal. This signal has the same magnitude as the positive signal that would have been created had we used a  $\pi/2$  pulse alone. With increasing pulse delay  $\tau$ , the negative signal corresponding to the  $T_1$  relaxation of the spin system is reduced. After time  $\tau_0$  the signal goes through zero since no further macroscopic population differences are observable. This corresponds to the transition from a negative spin temperature through "finite" to a positive spin temperature. As the time  $\tau$  further increases, the now positive signal approaches the value that would have been observed after the sole application of a  $\pi/2$  pulse. A similar experiment can be described by two  $\pi/2$  pulse using equ. (4.20). The time development of the  $\pi$ - $\pi/2$  experiment (*inversion recovery experiment*) of Fig.4.6 obeys the equation

$$n = n_{\text{thermal equilibrium}} \left( 1 - 2e^{-\frac{\tau}{T_1}} \right). \quad (4.23)$$

By setting the parentheses in equ. (4.23) equal to zero, we get  $\tau_0 = T_1 \ln 2$  as the passage of zero. From that we have a simple procedure to determine  $T_1$ , which, however, requires good adjustment of the pulse lengths and a homogenous high frequency field.

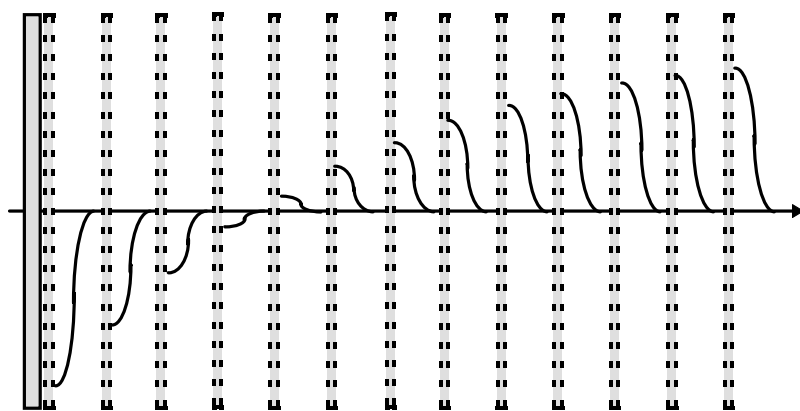


**Fig. 4.6** The inversion recovery experiment for the determination of  $T_1$ .

As an example for the calculation of relaxation times, we consider a homo-nuclear two spin system (nuclear separation  $r$ ) of a molecule in a liquid. We will neglect intermolecular nuclear magnetic interaction. Every spin is affected by the external magnetic field, which is superimposed with the  $z$ -component of the dipole-dipole interaction of neighboring atoms (this fluctuates due to molecular motion). A time- $(t)$ -independent correlation function  $G(\tau)$  of a function  $f(t)$  describes the magnetic interaction:

$$G(\tau) = \langle f(t)f(t+\tau) \rangle. \quad (4.24)$$

The pointy brackets in equ. (4.24) refer to the ensemble average over all particles. In chapter 8 of the classic NMR textbook of A. Abragam, it is shown that in the special case of rotational diffusion an exponential approach applies to a good approximation, from which the correlation time  $\tau_c$  is defined:

$$G(\tau) = G(0) \exp\left(-\frac{|\tau|}{\tau_c}\right). \quad (4.25)$$

If you imagine, for example, that a large molecule is reoriented by collisions with neighboring molecules,  $\tau_c$  is approximately the average time in which the molecule has reoriented itself through the solid angle 1. With the approach of (4.25), we get for  $T_1$  (see Abragam, p. 300)

$$\frac{1}{T_1} = \frac{1}{5} \frac{\gamma^4 \hbar^2}{r^6} \frac{I(I+1)}{4\pi\epsilon_0} \left( \frac{2\tau_c}{1+(\omega_L \tau_c)^2} + \frac{8\tau_c}{1+(2\omega_L \tau_c)^2} \right) \quad (4.26)$$

and for the transversal relaxation time  $T_2$

$$\frac{1}{T_2} = \frac{1}{5} \frac{\gamma^4 \hbar^2}{r^6} \frac{I(I+1)}{4\pi\epsilon_0} \left( 3\tau_c + \frac{5\tau_c}{1+(\omega_L \tau_c)^2} + \frac{2\tau_c}{1+(2\omega_L \tau_c)^2} \right). \quad (4.27)$$

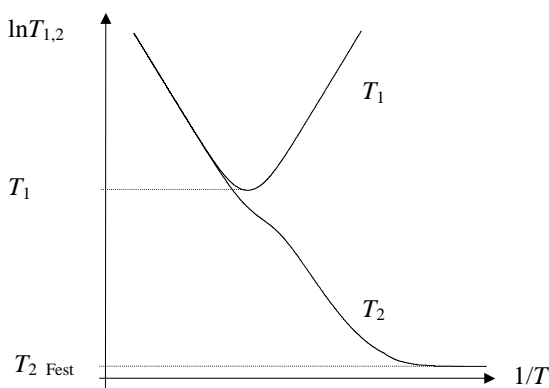


**Fig. 4.7** The relaxation times  $T_1$  and  $T_2$  as a function of the reciprocal absolute temperature  $1/T$  for a two spin system with *one* correlation time. Their temperature independency can be described by  $\tau_c = \tau_0 \exp(E_a/kT)$ .

It thus holds that  $T_1 = T_2 \propto 1/\tau_c$  when  $\omega_L \tau_c \ll 1$  and  $T_1 \propto \omega_L^2 \tau_c$  when  $\omega_L \tau_c \gg 1$ . Equ. (4.26) has a minimum of  $T_1$  at  $\omega_L \tau_c \approx 0,612$  or  $\nu_L \tau_c \approx 0,1$ . Thus, if we measure the relaxation time  $T_1$  of a two spin system at the Larmor frequency  $\nu_L$  as a function of the temperature and observe a minimum corresponding to equ. (4.26), we get the characteristic parameter  $\tau_c \approx 1/(10\nu_L)$  at the corresponding temperature. In the case at hand we can also measure an activation energy  $E_a$  of the correlation time, i.e. the rotational reorientation, from the linear branches of fig. 4.7.

If we have to consider *anisotropic* rotational diffusion or *multiple correlation times* in the characterization of a system, or if we can't use an *exponential function* for the temperature dependency, then the temperature development of the relaxation times in a liquid gets much more complicated. In Fig. 4.7,  $T_2$  becomes a constant at low temperatures (dotted line). This results from the fact that equ. (4.27) only applies if  $\tau_c < T_2$ . If  $\tau_c$  surpasses the value given by equ. (4.27), we see behavior resembling that of a solid body in the NMR spectrum, with a temperature independent value of  $T_2$ .

Since we have already discussed the temperature dependency of the transversal relaxation time  $T_2$ , we will now explain the cause of this relaxation. We will start with a phenomenological explanation of relaxation effects which assume that the reconstruction of a magnetization differing from static equilibrium in the  $z$ -direction is described by the relaxation time  $T_1$ , and  $T_2$  describes the decay of the transversal component of the magnetization in the  $x$ - $y$ -plane.

To derive the equations introduced by Felix Bloch into nuclear resonance (and later also into non-linear optics), we add two relaxation terms to equ. (4.13) and take the high frequency field  $B_{\text{rf}}$  into account. We get into the so-called "rotating" coordinate system, which rotates with the angular frequency  $\omega$  around the  $z$  axis of the laboratory coordinate system. The direction of rotation is mathematically positive when the gyromagnetic ratio  $\gamma$  is negative and negative if the ratio is positive. The unit vectors of the rotating system are  $e_x, e_y, e_z$ . The high frequency field is input with a coil in the  $x$ -direction of the laboratory coordinate system with the frequency  $\omega$  and amplitude  $2B_{\text{rf}}$ . This linear polarized field can be described by two circular polarized fields which rotate with the frequency  $\omega$  in the positive and negative sense around the  $z$  axis. From that we get an  $x$ -component  $B_{\text{rf}}$  in the rotating coordinate system which is time-independent at stationary input of high frequency ( $c\omega$  input). Instead of the external magnetic field, the only action in the rotating coordinate system is the magnetic induction of the resonance deviation  $(\omega_L - \omega)/\gamma$ , the "offset" or "resonant offset". If for the spins under study the input high frequency is identical to the Larmor frequency  $\omega_L = |\gamma B_0$ , the offset disappears. The effective working field in the rotating coordinate system is a vector addition of the rf field and the offset

$$\mathbf{B}_{\text{eff}} = (B_{\text{rf}}, 0, B_0 - \omega/\gamma). \quad (4.28)$$

With that we get the Bloch equations

$$\frac{d\mathbf{M}}{dt} = \gamma \mathbf{M} \times \mathbf{B}_{\text{eff}} - \frac{M_x \mathbf{e}_x + M_y \mathbf{e}_y}{T_2} - \frac{(M_z - M_0) \mathbf{e}_z}{T_1}. \quad (4.29)$$

$M_0$  is the equilibrium magnetization introduced in equ. (4.09), which adjusts itself for any starting condition after the switching off of the rf field and the dying out of the  $T_1$ -relaxation in the  $z$ -direction. Stationary solutions to the Bloch equations are attained for  $d\mathbf{M}/dt = 0$ . They are

$$\begin{aligned} M_x &= \frac{(\omega - \omega_L) T_2^2}{1 + (\omega - \omega_L)^2 T_2^2 + \gamma^2 B_{\text{HF}}^2 T_1 T_2} \gamma B_{\text{HF}} M_0 = 2\chi' H_{\text{HF}}, \\ M_y &= \frac{T_2}{1 + (\omega - \omega_L)^2 T_2^2 + \gamma^2 B_{\text{HF}}^2 T_1 T_2} \gamma B_{\text{HF}} M_0 = 2\chi'' H_{\text{HF}}, \\ M_z &= \frac{1 + (\omega - \omega_L)^2 T_2^2}{1 + (\omega - \omega_L)^2 T_2^2 + \gamma^2 B_{\text{HF}}^2 T_1 T_2} M_0. \end{aligned} \quad (4.30)$$

$\chi = \chi' - i\chi''$  was introduced as the complex susceptibility of the high frequency field. In the *cw*-procedure, a weak rf field is usually used to prevent saturation. The conditions for this are

$$\gamma^2 B_{\text{rf}}^2 T_1 T_2 \ll 1. \quad (4.31)$$

In this case (no saturation) the solutions of the Bloch equations simplify considerably, e.g.  $M_z = M_0 = \chi_0 H_0$ , see equ. (4.10).  $\chi'$  and  $\chi''$  no longer depend on the rf field.

The power absorbed by the spin system is the value averaged over one period of rotation in the laboratory coordinate system. It can be electronically measured in the sample coil.

$$P = -\mathbf{M} \cdot \frac{d\mathbf{B}_{\text{HF}}}{dt} \quad (4.32)$$

The rf field is linearly polarized there and only has an  $x$  component  $2B_{\text{rf}} \cos \omega t$ , whose time derivative is  $-2\omega B_{\text{rf}} \sin \omega t$ . We are therefore only interested in the  $x$  component of  $\mathbf{M}$ . After transformation into the laboratory coordinate system we get

$$M_x(t) = 2B_{\text{rf}}(\chi' \cos \omega t + \chi'' \sin \omega t)/\mu_0. \quad (4.33)$$

In the product  $-M_x dB_{\text{rf}}/dt$  only the term with  $\sin^2 \omega t$  remains after averaging over the period of rotation, which, when averaged over time, has a value of  $1/2$ . The absorbed power is

$$P = 2 \omega_L B_{\text{rf}}^2 \chi''/\mu_0. \quad (4.34)$$

It can be seen in equ. (4.34) that the line form of the absorption signal, which was measured as absorbed power over input frequency (or as Fourier transform of the free induction), depends on the imaginary part of the susceptibility. Due to the weak rf input, we get from equ. (4.30)

$$\chi'' = \frac{1}{2} \frac{T_2}{1 + (\omega - \omega_L)^2 T_2^2} \gamma \mu_0 M_0. \quad (4.35)$$

This gives us a Lorentz line form, which we recognize from equ. (2.71) or Fig. 2.5 in chapter 2.6. It is typical in NMR for spin systems influenced by motion. The half-width  $\delta\nu_{1/2}$  is called the full width at half maximum (fwhm), and is shown in Fig. 2.5. From equ. (4.35) we get

$$\delta\nu_{1/2} = \frac{1}{\pi T_2}, \quad (4.36)$$

from which the transversal relaxation time is brought into connection with the line width. Along the same lines that gave  $T_1$  the name spin-lattice relaxation time,  $T_2$  is called the spin-spin relaxation time. For example, in a solid body, the dipole-dipole interaction between two nuclear spins is the most important cause of line broadening for nuclei where  $I = 1/2$ . At the location of the nucleus under consideration, the dipoles of neighboring nuclei create an extra field  $B^{\text{Local}}$ , so that the resonance frequency of the nucleus is  $\nu = (B_0 + B_z^{\text{Local}}) \gamma/2\pi$ . If we again consider the homo-nuclear two spin system with the inter-atomic distance  $r$  and the angle  $\theta$  between  $\mathbf{r}$  and  $\mathbf{e}_z$ , then we get

$$\Delta\omega = \pm \frac{3\gamma_1^2 \hbar}{2r^3} \frac{\mu_0}{4\pi} \frac{3\cos^2 \theta - 1}{2} \quad (4.37)$$

for the resonance shift caused by the dipolar interaction in the solid body where  $m = \pm 1/2$  is the state of the neighboring spin.

In powder samples, the orientations of the inter-atomic vectors to the external magnetic field are statistically distributed. The term  $3\cos^2\theta - 1$  in equ. (4.37) assumes values between 2 and  $-1$ . Thus a broadening of the resonance line occurs. In liquids, through the rapid reorientation of the inter-atomic vectors, the local fields are averaged out and the line narrowing is inverse proportion to  $\tau_c$  (extension of  $T_2$  with increasing temperature in Fig. 4.7). From equations (4.34-36) it can be immediately seen that as the line is narrowing (extension of  $T_2$ ), the maximum absorption and thus the signal height grows, but the integral over the function stays constant.

A narrowing of the solid body signal can be reached by rapid rotation of the sample around the magic-angle (magic-angle spinning, MAS). For the magic-angle  $\arccos 3^{-1/2} \approx 54,74^\circ$  the geometry dependent factor in equ. (4.37) becomes zero, i.e. a dipole-dipole interaction at this angle to the external magnetic field does not cause resonant shifting. It is now necessary to average out the dipole-dipole interactions perpendicular to this direction. This is accomplished by rapid rotation of the sample around an axis that includes the magic-angle with the external magnetic field. We can thereby drastically reduce the dipole-dipole broadening of a solid body signal, if the rotation frequency is greater than the width of the spectra given by equ. (4.37). The air powered rotors normally reach frequencies between 2 and 40 kHz.

Beside the homo-nuclear dipole-dipole interaction, there are other causes which lead to resonance shifting with the geometry factor  $3\cos^2\theta - 1$ : heteronuclear interaction, anisotropy of the chemical shift (see chapter 4.4), and quadrupole interaction (the nuclear quadrupole moment for  $I < 1/2$  with the electric field gradient tensor *with respect to the first order*). The broadening of the signals of powder samples as a consequence of these interactions can also be averaged out by means of MAS. Besides the increase in detection sensitivity resulting from the narrowing of lines, an more exact determination of the resonant frequency and the value of the chemical shift is obtained, see chapter 4.4. Rapid sample rotation has become a fundamental technology in solid-state NMR.

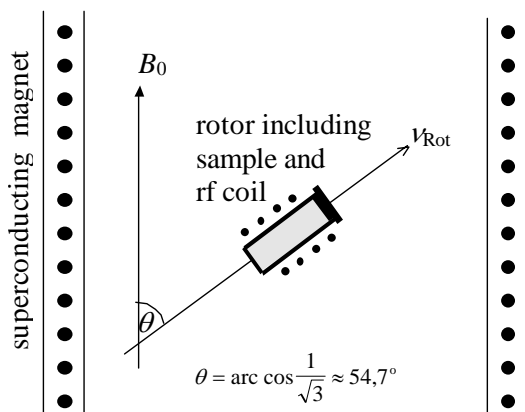


**Fig. 4.8** The rapid rotation of the sample around the magic-angle. The stator (not shown) contains the rf coil and the jets for the air bearings and drive, which are arranged diagonally against small grooves in the cap of the rotor.

In the discussion of detector sensitivity, we consider the signal-to-noise ratio (SNR) of a line in an absorption spectrum. The magnitude of the signal is the maximum amplitude of the signal  $f_{\max}$ . For the magnitude of the noise we use the standard deviation  $\sigma$  of the measured signal from zero away of the resonance. The maximum attainable signal to noise ratio is influenced by the density of nuclei  $N$ , the external magnetic field  $B_0$ , the absolute temperature  $T$ , the gyromagnetic ratio  $\gamma$ , the nuclear spin  $I$ , the relaxation times  $T_1$ ,  $T_2$ , and the measurement time  $t_{\text{meas}}$  in the following way:

$$\text{SNR} \propto N \gamma^{5/2} B_0^{3/2} T^{-3/2} I(I+1) \sqrt{\frac{T_2}{T_1}} \sqrt{t_{\text{meas}}} \quad (4.38)$$

The proportionality to  $N$  is due to the fact that the magnetization is the sum of nuclear moments per unit volume. The equ. (4.09) in chapter 4.1 (equilibrium magnetization) contains the factors  $I(I+1)\gamma^2 B_0^1 T^{-1}$ . In the derivation of equ. (4.34) we see that the measurable power in the rf coil is proportional to  $\omega_L$ , from which follows an additional proportionality of the SNR to  $\gamma^1 B_0^1$ . The frequency and temperature dependence of the electronic noise is given by  $\sqrt{\omega T}$  (white noise per definition). From that we get the extra factors  $\gamma^{-1/2} B_0^{-1/2} T^{-1/2}$  in the SNR. This explains the powers of  $\gamma$ ,  $B_0$  and  $T$  in equ. (4.38).

The detection of nuclear resonances is always done by the observation of one component of the macroscopic magnetization in the  $x$ - $y$ -plane (preferably after a  $\pi/2$  pulse). This component rotates around the  $z$ -axis at the Larmor frequency and can be observed as induction in the coil in the  $x$ -direction before it decays after a time on the order of the transversal relaxation time  $T_2$ . If we want to conduct a new NMR experiment afterwards, we have to wait for a time on the order of the longitudinal relaxation time  $T_1$ , before the macroscopic magnetization has returned to its equilibrium state in the  $z$ -direction. We could then apply a  $\pi/2$  pulse, watch the free induction, and add the new signal to the one we already have in the computer. This signal accumulation process is continually repeated during the measurement period  $t_{\text{meas}}$  of a few minutes to days. The sum of the effective observation time is then  $(T_2/T_1)t_{\text{meas}}$ . The number  $n$  of statistically independent measurement points increases in proportion to the effective observation time. The signal is overlaid with a normal distribution error by the electronic noise. From error calculations it is known that the average value of  $n$  measurements only differs on average from the true value by

$$\Delta\bar{x} = \frac{\sigma}{\sqrt{n}}. \quad (4.39)$$

The factors  $\sqrt{T_2/T_1} \sqrt{t_{\text{meas}}}$  in equ. (4.38) are thus explained. With  $n$  signal accumulations where  $n = t_{\text{meas}}/T_1$ , these factors can be replaced with  $\sqrt{T_2} \sqrt{n}$ , whereby the dependency on the number of scans can be better demonstrated.

In equ. (4.38),  $\gamma^{5/2}I(I+1)$  represents a quantity which only depends on the location of the nuclei. It tells us the "relative sensitivity" of different nuclei in the same field. If we set the numerical value to 1 for  $^1\text{H}$ , then, using the same number of nuclei used in  $^1\text{H}$ , and with the same field strength (but naturally different Larmor frequencies), we get a measurement sensitivity of 0,016 for  $^{13}\text{C}$ ,  $10^{-3}$  for  $^{15}\text{N}$ , 0,83 for  $^{19}\text{F}$ , 0,1 for  $^{23}\text{Na}$ , 0,2 for  $^{27}\text{Al}$  and 0,01 for  $^{29}\text{Si}$ . More exact numerical values for these and other nuclei can be calculated from the values in Tab. 4.1.

The value given here for  $^{13}\text{C}$  is further reduced if we have to make do with the natural abundance of  $^{13}\text{C}$  nuclei (1,11%). Despite this sensitivity disadvantage, this nucleus is studied almost as often as the  $^1\text{H}$  nucleus. It is caused on the one hand by the central role of carbon in chemistry and on the other hand by the more simple spectrum, since the number of carbon atoms is mostly smaller than the number of hydrogen atoms in organic compounds.

Before we move on to the section on chemical shifts, we want to clarify a difference between solid-state and liquid NMR.  $T_1/T_2$  is about one for liquids, as can be seen in the equations (4.26-27) when  $\omega_L \tau_c \ll 1$ . In solid bodies, it is possible for the quotient  $T_1/T_2$  to assume values up to  $10^8$ . This results in a reduced detection sensitivity of up to  $10^{-4}$  times, as calculated from equ. (4.38).

#### 4.4 Chemical Shift

The external magnetic field  $B_0$  can only affect a nucleus without shielding, if the atom has been stripped of its electrons. Through the action of the electron shell, the magnetic field at the nucleus is changed. This can be understood by imagining that, when the magnetic field is turned on, an opposing current is induced in the spherical electron shell of the s orbital. This produces an extra (diamagnetic) field which opposed the external field. If the valence electrons are not in the spherically symmetric p orbitals, then the external field affects the electron shell in such a way that a field proportional and co-directional to the external field is created, thus resulting in paramagnetic shift. The resulting field  $B_0'$  at the nucleus is described by a screening constant  $\sigma$

$$B_0' = (1 - \sigma)B_0. \quad (4.40)$$

The charge distribution of the bonding electrons is affected by the chemical bonds. For this reason, the effect of the shift of the nuclear magnetic resonance is called the *chemical shift*. The screening constant  $\sigma$  is only still used in theoretical considerations. The reason is that the resonance frequency of the bare nucleus is not appropriate as a point of reference, because it is not experimentally measurable. Instead of that, an easily measurable reference substance is used to define the dimensionless value, usually given in *parts per million* (ppm,  $10^{-6}$ ), of the chemical shift  $\delta$

$$\delta = \sigma_{\text{Reference}} - \sigma. \quad (4.41)$$

Reference substances are usually standard by convention, e.g. TMS (tetramethylsilane,  $\text{Si}(\text{CH}_3)_4$ ) for the three nuclei  $^1\text{H}$ ,  $^{13}\text{C}$  and  $^{29}\text{Si}$  NMR. Take note that when using the chemical shift  $\delta$  instead of magnetic screening  $\sigma$ , the sign is changed: *A positive chemical shift  $\delta$  indicates less screening and a correspondingly higher resonance frequency at the same external field  $B_0$ .*

The distribution of the electron density is not, in general, isotropic. For this reason, both screening and chemical shift are tensors by nature. In NMR studies on solids, it is possible to measure different screening along the main axes of the bonding system. In liquids, molecular units reorient themselves so quickly that only the average value of the screening is observable, i.e. the characteristic isotropic screening or isotropic chemical shift given by the trace of the screening tensor.

In the  $^1\text{H}$  NMR, the diamagnetic contributions of the screening dominate. In other nuclei, paramagnetic contributions can take precedence. If multiple bonds occur in the vicinity, separation into diamagnetic and paramagnetic components is questionable. Classical calculations can, at best, describe a diamagnetic shift. Semi-empirical quantum chemical calculations of screening are not free of random assumptions, so that the ab-initio calculation of quantum chemistry is often used to calculate the chemical shift. Due to the enormous amount of experimental data for chemical shifts, it is rarely necessary to use calculated values for the interpretation of spectra. Nevertheless, the calculation of chemical shifts has remained a fundamental problem in theoretical works. On the other hand, quantum mechanical calculations can be tested against the measured values of the screening constant.

The size of the  $\delta$  scale covered by the individual nuclei in different molecules increases with the electron shell. In  $^1\text{H}$  nuclei, about 20 ppm of the  $\delta$  scale is covered, in  $^{13}\text{C}$  about 400 ppm, and in  $^{205}\text{Tl}$  about 10 000 ppm. The chemical shifts of nuclei in liquid substances have been collected in reference works, although the use of books is being rapidly replaced by the use of computer data bases.

In Fig. 4.4, the  $^1\text{H}$  NMR spectrum of ethanol is shown. It contains three signal groups: the relative intensities of these signal groups can be obtained by integration of the spectrum over the range of the signal group. If we define the relative intensity of the triplet of the  $\text{CH}_3$  group at 1,18 ppm to the value of 3, then the quartet of the  $\text{CH}_2$  group at 3,59 ppm gives the relative intensity 2, the singlet of the  $\text{OH}$  group has to have a relative intensity of 1. The latter signal occurs through the exchange of the OH protons with the protons of the solvent water, whose chemical shift is 4,78 ppm. Due to a small residual concentration of  $\text{H}_2\text{O}$  in the solvent  $\text{D}_2\text{O}$ , the relative intensity of the singlet is somewhat greater than 1. The splitting of the signals of the  $\text{CH}_2$  and  $\text{CH}_3$  groups by scalar coupling will be explained in chapter 4.5.

The chemical shifts of special groups in molecules, e.g. the  $\text{CH}_3$  groups, depend on the rest of the molecule. In addition, the chemical shifts also depend on the solvent, i.e. the neighboring molecules. Table 4.2 shows the chemical shifts of  $^1\text{H}$ ,  $^{13}\text{C}$ ,  $^{15}\text{N}$ ,  $^{17}\text{O}$ ,  $^{19}\text{F}$ , and  $^{31}\text{P}$  resonances of selected molecules in a liquid, in a solvent (with minimal intermolecular interactions with the molecule), or in the gas state. The usual reference substances and the size of ranges of the chemical shifts for a few substances are given in Fig. 4.9.

**Table 4.2** Chemical shifts of various nuclei in liquid and vapor bonds. The shifts for each nuclear location are relative to the reference substances shown in Fig. 4.9 and are shown in the order in which they are found in the formula. The state "in solution" usually refers to a strong dilution in  $\text{CCl}_4$  or  $\text{CDCl}_3$ .

Name	State	Formula	Chemical Shift in ppm
ammonia	gas	$\text{NH}_3$	0,09
acetonitrile	liquid	$\text{CH}_3\text{CN}$	0,3/2,0/117,2/-136,4
benzene	in solution	$\text{C}_6\text{H}_6$	128,5/7,26
benzene	liquid	$\text{C}_6\text{H}_6$	128,7/7,4
butane	in solution	$\text{CH}_3\text{CH}_2\text{CH}_2\text{CH}_3$	13,0/0,90/24,8/1,23
(E)-2-butene	in solution	$\text{CH}_3\text{CHCHCH}_3$	16,8/1,63/125,4/5,43
(Z)-2-butene	in solution	$\text{CH}_3\text{CHCHCH}_3$	11,4/1,60/124,2/5,45
1-butene	in solution	$\text{CH}_2\text{CHCH}_2\text{CH}_3$	113,5/4,9/140,5/5,79/27,4/2,00/13,4/1,01
ethylene	in solution	$\text{CH}_2\text{CH}_2$	123,3/5,28
isobutene	in solution	$\text{CH}_2\text{C}(\text{CH}_3)_2$	111,3/4,80/141,8/24,2/1,70
methane	in solution	$\text{CH}_4$	-2,3/0,23
Nitromethane	liquid	$\text{CH}_3\text{NO}_2$	57,3/4,3/0,0/605
propane	in solution	$\text{CH}_3\text{CH}_2\text{CH}_3$	16,0/0,91/16,3/1,33
water	liquid	$\text{H}_2\text{O}$	4,79/0,0
water	gas	$\text{H}_2\text{O}$	0,31/-36,10
hydrogen	gas	$\text{H}_2$	4,34
tetrafluormethane	Liquid	$\text{CF}_4$	123,6/-63,4
hydrofluoric acid	solution	$\text{HF}$	1,85/-221

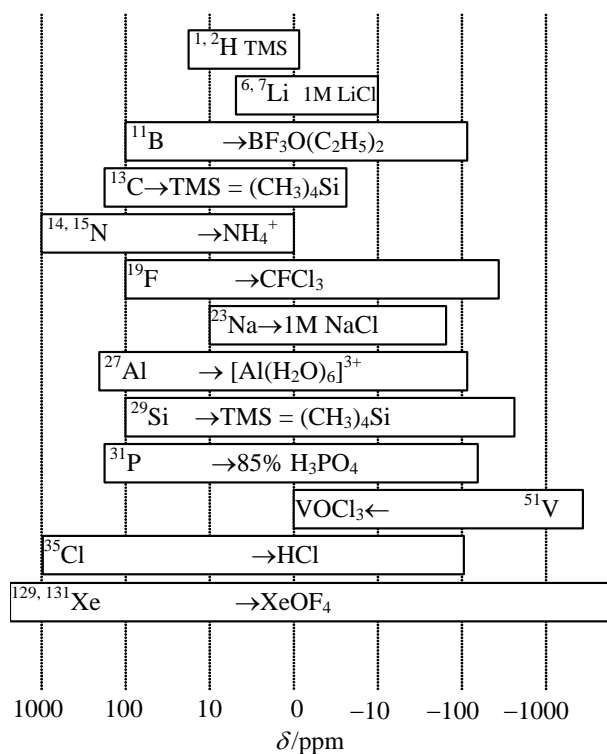


**Fig. 4.9** Ranges of the chemical shifts of a few nuclei and the reference substances, relative to which each shift is related.

The chemical shifts of nuclei in solid bodies are more difficult to determine experimentally. Through the use of the MAS technique described in chapter 4.3, it has been possible for a few years to narrow most solid body signals to such a degree that sufficiently accurate determination of the resonance position is possible. Only the isotropic part of the chemical shift (trace of the screening tensor) is usually measured in liquids. With that, the measurement of the  $\delta$  parameter is also of great importance in solid-state NMR experiments.

Figure 4.10 shows the  $^{29}\text{Si}$  MAS NMR Spectrum of the highly porous crystalline material silicalite, is composed of an  $\text{SiO}_2$  frame with 24 different Si positions per elementary cell, see right. At these locations, the tetrahedral silicon surrounded by oxygen has slightly different bonding angles and bonding lengths, which result in the observed differences in the chemical shifts.

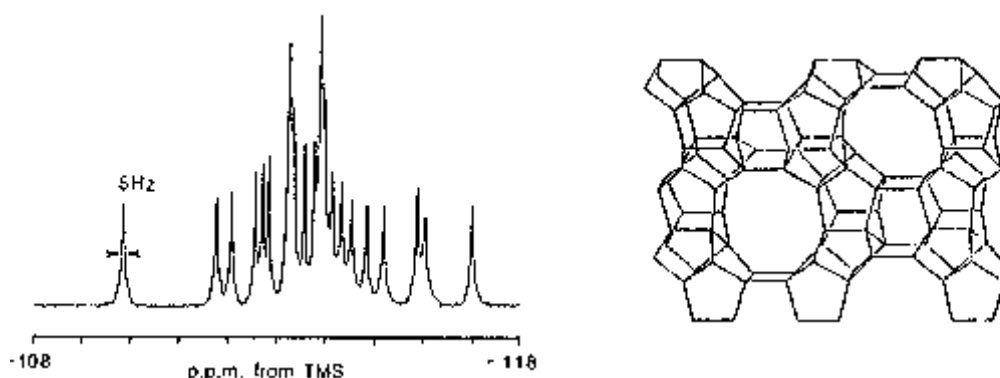


**Fig. 4.10**  $^{29}\text{Si}$  MAS NMR Spectrum of the zeolite ZSM-5, Fyfe et al Nature 326 (1987) 281

## 4.5 Scalar Spin-Spin Interaction

Let us return to Fig. 4.4 to explain the splitting of the signal of the CH<sub>3</sub> and CH<sub>2</sub> groups in the ethanol spectrum into a triplet and quartet. This fine structure of the spectra is caused by indirect spin-spin coupling. Synonymous references are *J* coupling and *scalar* coupling. In opposition to this, there is also the previously mentioned *dipole-dipole* interaction, which leads to the broadening of solid body lines over a direct spin-spin coupling. Equation (4.27) and Fig. 4.7 show that the influence of direct dipole coupling in liquids decreases with reducing correlation times and increasing temperature. This is not true for scalar interactions, however. The source of scalar coupling is a direction independent polarization mechanism in which the nuclear magnetization between neighboring nuclei is transferred by bonding electrons.

Before we explain the effect, two important characteristics should be mentioned. The first is that the scalar interaction causes a splitting which does not usually depend on the external magnetic field. The coupling constant *J* is given in Hz. In contrast, giving the chemical shift in frequency units would be a quantity dependent on the external magnetic field. Therefore,  $\delta$  is given as a frequency shift per resonant frequency in the dimensionless unit ppm. The second characteristic is that equivalent nuclei do not split each other. Aside from belonging to the same isotope and having the same chemical shift, the equivalence of nuclei in a group requires that all other nuclei of the molecule (regardless of whether these have nuclear spin) have the same coupling to all the nuclei of the group. It follows from geometry considerations alone that, for example, the <sup>1</sup>H nuclei of methane, but also the two <sup>1</sup>H nuclei (and the two <sup>19</sup>F nuclei) in CH<sub>2</sub>F<sub>2</sub> are equivalent. The corresponding nuclei in C<sub>2</sub>H<sub>2</sub>F<sub>2</sub> are non-equivalent, since the two carbon nuclei have unequal distances to the nuclei of the group. A different circumstance is seen in ethanol: due to the quick rotation around the C-C bonds, the <sup>1</sup>H nuclei in the CH<sub>2</sub> group are equivalent, as are those in the CH<sub>3</sub> group. The splitting occurs through the *J* coupling between the CH<sub>3</sub> and CH<sub>2</sub> protons. Accordingly, we get a triplet for the CH<sub>3</sub> protons. The COH proton is further away and also usually replaced by a deuterium nucleus. It therefore has no influence on the splitting of the CH<sub>2</sub> protons.

Let us now consider the simplest case of <sup>1</sup>*J*<sub>AX</sub> coupling of two spin ½ nuclei A and X, which are bonded by an electron pair. The number of bonds between neighboring atoms is written in the notation <sup>1</sup>*J*<sub>AX</sub> in the preceding index, and the suffix index symbolizes non-equivalent nuclei. In Fig. 4.11, the physical basis of the scalar coupling is clarified. A nucleus-electron interaction occurs through the dipolar interaction between nuclear spin and a non-spherical electron orbital, or through Fermi contact interaction resulting from the non-disappearing electron charge at the nucleus for s orbitals. Between a nucleus and a bonding electron associated with the nucleus, a parallel (or in some instances anti-parallel) orientation of the *I* and *S* spins (nuclear and electron spin, respectively) is energetically preferred. The electron spins of the bonding electrons associated with the two nuclei are strongly correlated. For s electrons, the Pauli principle demands that the spins of electron pairs be opposed.

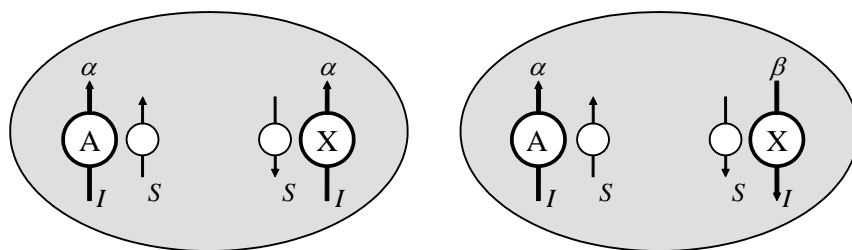
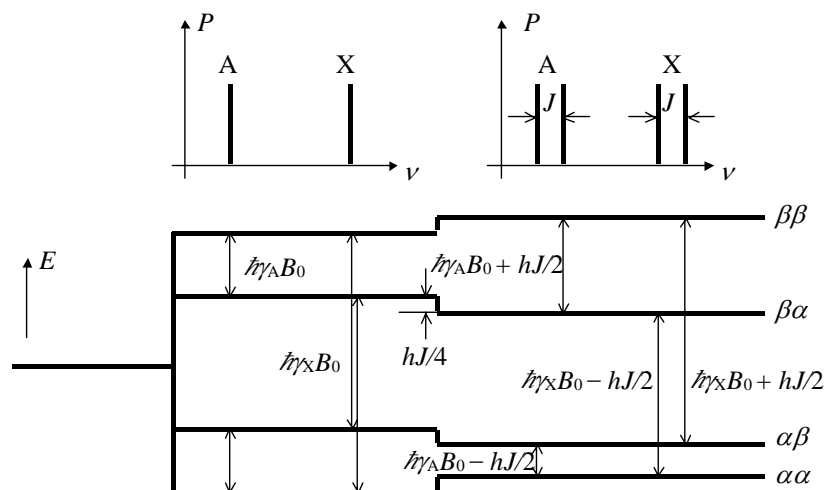


**Fig. 4.11** Representation of the parallel ( $\alpha\alpha$ ) and anti-parallel ( $\alpha\beta$ ) orientations of two nuclear spins  $I$  in the nuclei A and X, which are coupled to the spins  $S$  through an  $s$ -electron pair.

In general in magnetic resonance, the spin state  $m = +1/2$  is called  $\alpha$  and the state  $m = -1/2$  is called  $\beta$ . Let us now consider two nuclei A and X with positive gyromagnetic ratios, where  $\gamma_X > \gamma_A > 0$ , in which a parallel arrangement of neighboring nuclear and electron spins should be energetically preferred. If we only consider the Zeeman energy, equ. (4.08) tells us that the state  $\alpha\alpha$  has the lowest energy and the state  $\beta\beta$  the highest. The scalar interaction shifts the energy levels in different ways: for the state  $\alpha\alpha$ ,  $m_{IA} = +1/2$  and  $m_{IX} = +1/2$ . The electron found near A should then have a parallel  $\alpha$  electron spin,  $m_{SA} = +1/2$ , since the corresponding electron prefers a location near this nucleus. Since both electron spins must be anti-parallel, it holds that  $m_{SX} = -1/2$ , thus the electron and nuclear spins of the X atom are anti-parallel, which is energetically disadvantageous. The scalar coupling therefore creates a small increase in the energy of the  $\alpha\alpha$  level. The state  $\alpha\beta$ , however, experiences a reduction in the energy level through spin-spin coupling. In the state  $\alpha\beta$  and  $\beta\alpha$  the nuclear and electron spins can be parallel in both nuclei. This is energetically preferred (lower energy). In the state  $\beta\beta$ , a parallel orientation of the electron spins to their neighboring nuclear spins is forbidden by the Pauli principle. This is why the energy of the  $\beta\beta$  state increases through  $J$  coupling by the same amount as the  $\alpha\alpha$ -state.

**Fig. 4.12** The AX two spin system ( $I = 1/2$ ). On the bottom we see the ground state (left), splitting by the Zeeman effect (middle) and the shift of the energy levels caused by  $J$  coupling (right). The corresponding absorption spectra are shown on the top.



In magnetic resonance transitions, only one magnetic quantum number  $m$  is changed. Four transitions are possible in our example, see Fig. 4.12. In the absence of  $J$  coupling, we get only one line at frequency  $\omega_A = \gamma_A B_0$  for the transitions  $\alpha\alpha \leftrightarrow \beta\alpha$  and  $\alpha\beta \leftrightarrow \beta\beta$ , and another at  $\omega_X = \gamma_X B_0$  for the two other transitions  $\alpha\alpha \leftrightarrow \alpha\beta$  and  $\beta\alpha \leftrightarrow \beta\beta$ . With  $J$  coupling, the Zeeman levels of the nuclei A and X are split, the singlets are replaced by doublets. The upper portion of Fig. 4.12 shows the spectra.

In an  $AX_2$  system, an A nucleus has two indistinguishable neighboring X nuclei. Analogous considerations lead to a triplet for the A resonance. In the line with the average frequency, one neighboring spin is parallel and the other antiparallel to the A spin. This variant has twice the probability of the cases where both spins are either parallel or anti-parallel. The intensities of the three lines are thus related as 1:2:1. These considerations can be continued for more than two equivalent neighbors. In general for the nuclear spin  $I = \frac{1}{2}$ , the resonance of a nucleus A in an  $AX_n$  system is split into  $n + 1$  lines, whose intensities can be taken from Pascal's triangle, see Fig 4.13.

$n$ , Number of Neighbors	Intensities of the $n + 1$ Lines							
0	1						singlet	
1	1 1						doublet	
2	1 2 1						triplet	
3	1 3 3 1						quartet	
4	1 4 6 4 1						quintet	
5	1 5 10 10 5 1						sextet	
6	1 6 15 20 15 6 1							septet

**Fig. 4.13** Intensity of the lines appearing in an  $AX_n$  bond. The signal of the resonant nuclei A is split by  $J$  couplings with  $n$  neighbors into a multiplet of equidistant individual lines (third column) of the given intensities.

The relationships in quadrupole nuclei ( $I > \frac{1}{2}$ ) are different. A quadrupole nucleus splits every line of its neighbor into  $2I + 1$  lines of equal intensity. A neighboring  $^2\text{H}$  nucleus causes a triplet just as two  $^1\text{H}$  nuclei would do, but the intensity relationships (1:1:1) and (1:2:1), respectively, make differentiation possible.

The  $J$  coupling is averaged out through molecular reorientation as a scalar spin-spin interaction, in contrast to vector dipole-dipole interaction. But sufficiently intense high frequency input at the Larmor frequency of the neighboring nucleus causes a rapid reorientation of the spin vector. This can lead to averaging out of both the scalar and vector spin-spin interactions. We will get into this "decoupling" in chapter 4.7. We will also demonstrate there how  $J$  coupling can be employed to find correlations between neighboring nuclei in two dimensional spectroscopy.

#### 4.6 Simplest Example of a Pulse Train: the Hahn Echo

In the early years of nuclear magnetic resonance, the homogeneity of the magnets was still relatively poor. The line forms of the signals of liquid substances were, in general, greatly broadened by this field inhomogeneity, or the free induction decay of the signal after a  $\pi/2$  pulse quickly decayed. Erwin L. Hahn demonstrated in 1950 that through the application of an additional  $\pi$  pulse after a delay  $\tau$ , a refocusing effect occurred on the macroscopic magnetization (which was defocused as a result of field inhomogeneity) of the spin system. This  $\pi/2$ - $\pi$  Pulse sequence for the production of the Hahn echo is still frequently used today, for example in the averaging out of interactions which produce inhomogeneous line broadening, for overcoming dead time problems in solid-state NMR, and in all processes dealing with pulsed field gradients.

We will clarify with the simplest model the action of the Hahn pulse group on a spin-spin system: a local magnetic field acts in addition to the external magnetic field, so that we have  $B_z = B_0 + \Delta B_z$ . From the laboratory coordinate system LAB we again move into the rotating coordinate system ROT, which rotates in the direction of the external magnetic field with the Larmor angular frequency  $\omega_L = \gamma B_0$ , which is *in resonance*. In this case, the influence of the external magnetic field  $B_0 = \omega_L/\gamma$  is no longer noticeable, in contrast to the local field which still is.

In the following, we assume that  $\tau_{\pi/2} \ll \tau$ ,  $\tau_{\pi/2}$  is set by  $\gamma B_{\text{HF}} \tau_{\pi/2} = \pi/2$ , and  $\tau$  is the delay between the two pulses. By applying a short  $\pi/2$  pulse, the magnetization at time  $t = 0$  flops from the  $z$ -direction into the perpendicular  $x$ - $y$ -plane. If the phase of the  $\pi/2$  pulse is so arranged that it corresponds with the  $y^{\text{ROT}}$ -direction of the rotating coordinate system, the macroscopic magnetization after the  $\pi/2$  pulse corresponds with the  $x^{\text{ROT}}$ -direction. In the absence of an additional local field and other nuclear resonant interactions, the  $x^{\text{ROT}}$  magnetization would be conserved and produce an undamped free induction decay of angular frequency  $\omega_L$  in the rf coil lying in the  $y_{\text{LAB}}$ -direction. Under the influence of the positive or negative  $z$ -component of the local field  $\Delta B_z$ , the magnetization of this nucleus now spins in the rotating coordinate system with the angular frequency

$$\Delta\omega = \gamma\Delta B_z \quad (4.42)$$

and builds a phase angle (with the  $x$ -direction of the rotating coordinate system)

$$\alpha(t) = \Delta\omega t. \quad (4.43)$$

A sample usually has areas which are subjected to different local fields. This is the case when the additional local field is caused by an inhomogeneity in the external magnetic field, or when an anisotropic chemical shift in a powder sample modifies the field acting on a nucleus.  $B_z$  and therefore also  $\Delta\omega$  and the phase angle  $\alpha$  assume different positive or negative values in these areas, and the macroscopic magnetization present after the  $\pi/2$  pulse in the  $x$ -direction rapidly decays. The partial magnetization in the different areas are, after a certain time, evenly distributed in all directions in the  $x$ - $y$ -plane, and no further signal is induced in the sample coil.

At time  $t = \tau$ , a  $\pi$  pulse is applied. It has twice the length of a  $\pi/2$  pulse, and its phase corresponds to the  $x$ -direction of the rotating coordinate system. The spin magnetization in all areas of the sample turns  $180^\circ$  around the  $x$ -axis of the rotating coordinate system. The sign of the phase angle  $\alpha$  is thereby reversed by the  $\pi$  pulse at time  $t = \tau$ . The spins continue to rotate in the  $x$ - $y$ -plane with  $\Delta\omega(r)$ , but for the phase angle we now have

$$\alpha(r,t) = -\alpha(r,\tau) + \Delta\omega(r) \cdot (t - \tau). \quad (4.44)$$

If, after the  $\pi$  pulse, we again wait for time  $\tau$ ,  $t = 2\tau$ . If we put this time into equ. (4.44) and compare to equ. (4.43), we see that  $\alpha(r,2\tau) = 0$ . With that, at time  $t = 2\tau$ , the total macroscopic magnetization which dissipated under the influence of the local field is refocused and again dissipates when  $t > 2\tau$ . In the rf coil, a signal is induced at time  $t = 2\tau$  which is an "echo" of the free induction decay (FID).

Although we used a  $\pi$  pulse in chapter 4.3 which, without a preceding a  $\pi/2$  pulse, resulted in the inversion of the occupation numbers and all nuclear moments, the  $\pi$  pulse sent after the  $\pi/2$  pulse in the Hahn echo produces an inversion of the coherences. In field inhomogeneities, heteronuclear dipolar interactions, scalar couplings, and chemical shifts, the amplitude of the echo corresponds to the starting amplitude of the free induction decay, as long as the time-variable spatial coordinates of the nuclei or the longitudinal relaxation do not cause damping.

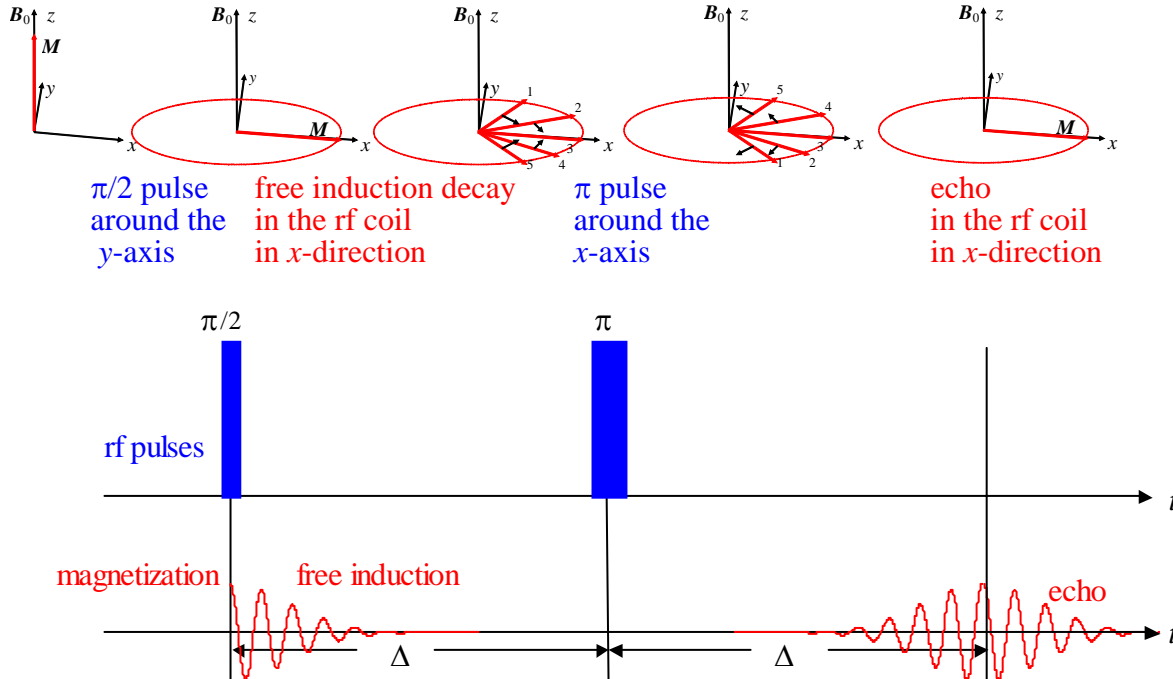


**Fig. 4.14** The Hahn echo: the magnetization in the magnetic field  $B_0$  under the influence of radio frequency pulses and a field inhomogeneity. The latter is labeled in the figure by five spatially separated areas 1 - 5 of the sample, which are in external fields  $B_0+2\delta$ ,  $B_0+\delta$ ,  $B_0$ ,  $B_0-\delta$  and  $B_0-2\delta$ . The static magnetization is rotated by the  $\pi/2$  pulse with phase  $y$  from the  $z$ -direction into the  $x$ -direction of the rotating coordinate system. Under the influence of the field inhomogeneity, the magnetizations in the different areas of the sample dissipate at different rates. The middle area 3 is in the field  $B_0$  in resonance with the frequency  $-\omega_L = \gamma B_0$  of the rotating coordinate system and therefore always points along its  $x$  axis. The areas 1 and 2 are in a higher field and the areas 4 and 5 are in a weaker field. Correspondingly, the spins in area 1 rotate with the angular frequency  $\Delta\omega = 2\gamma\delta$  faster, and those in area 5 by the same amount slower as the angular frequency of the rotating coordinate system. The  $\pi$  pulse, which is applied with phase  $x$  at time  $\tau$  after the first pulse, rotates the magnetization of all areas of the sample by  $180^\circ$  around the  $x$ -axis. The signs of the phase differences  $\Delta\omega t$  developing with time  $t$  are thereby reversed. After the  $\pi$  pulse, the phase differences continue to develop with  $\Delta\omega t$ , since the field homogeneity is constant in time. Therefore, all spin packets are focused in the  $x$ -direction of the rotating coordinate system after a time  $2\tau$  Hahn spin echo occurs.

The Hahn echo corresponds in size and form to the (additionally mirrored) free induction decay (FID). It only has the size of the initial value of the FID if neither

- a normal  $T_2$  relaxation or
- a diffusion of the nuclei has occurred.

The Hahn echo gives us the ability to cancel the influence of magnetic field inhomogeneities (as well as the heteronuclear dipole-dipole interaction, the anisotropy of the chemical shift, etc.) on the  $T_2$  relaxation. In addition, we can measure the diffusion and self-diffusion coefficients of molecules by applying a strong field gradient (may be pulsed).

## 4.7 Two Dimensional NMR, Decoupling, Double Resonance

A one dimensional spectrum displays absorption as a function of resonant frequencies (usually as a  $\delta$ -scale). It can be calculated from the time dependent free induction decay (FID) using one-dimensional Fourier transformation, as shown in chapter 4.2. Two dimensional spectra represent the absorption as a function of two quantities, for example the chemical shift and the  $J$ -coupling, or the chemical shift of two nuclei. The spectra with the two frequency scales  $\omega_1$  and  $\omega_2$  are obtained from a two-dimensional Fourier transformation with respect to two independent variable times  $t_1$  and  $t_2$ .

Decoupling is used to eliminate the influence of other nuclei on the nucleus to be examined. This involves inputting the resonant frequency of the other nuclei during signal measurement of the nucleus in question, which leads to frequent level transitions in the nuclear spins of the other nuclei.

Multiple resonances require the input of multiple nuclear resonance frequencies during an experiment. Double resonance is present in a limited sense, when by simultaneously irradiation of two nuclei, e.g.  $^1\text{H}$  and  $^{13}\text{C}$ , with the two correspondent Larmor frequencies, we get polarization transfer or coherence transfer between the two spin systems. In a simplified picture, the polarization corresponds to the magnetization of the undisturbed external magnetic field in the  $z$ -direction (different populations of the Zeeman levels), and the coherence corresponds to the transversal magnetization after a  $\pi/2$  pulse. In quantum mechanics, the population probabilities are described by the diagonal elements and the transitions (coherences) by the elements in the first sub-diagonal of the spin density matrix.

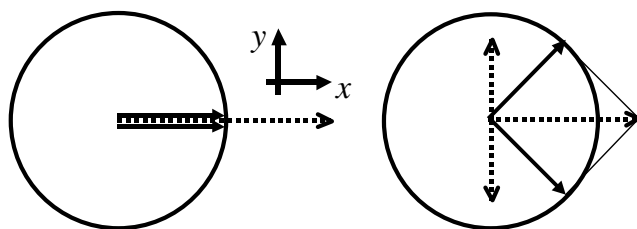


**Fig. 4.15** Creation of anti-phase coherence of  $I$  spins ( $I = 1/2$ ) under the influence of a  $J$  coupling of the  $I$  spins with neighboring spins ( $S = 1/2$ ). The figure shows  $t = 0$  on the left hand side and  $t = 1/4J$  on the right.

Coherence transfer requires the creation of an anti-phase coherence, which occurs by  $J$ -coupling of two spins. Figure 4.15 shows how  $I_x$  becomes  $I_x \cos \pi J t + 2I_y S_z \sin \pi J t$ , in which the anti-phase coherence occurs because  $S_z = \pm 1/2$  ( $\alpha$  and  $\beta$  settings of the  $S$  spins are approximately equally probable). This transition can also be described using product operator formalism. It has a function in NMR similar to that of complex alternating current calculations in electronics. We can allow ourselves to ignore the theoretical background if we know the rules. The most important transformations of product operators under the influence of pulses, scalar coupling, and chemical shifts can be written down in a few lines (see for example Ernst, Bodenhausen, Wokaun or the original O.W. Sørensen, G.W. Eich, M.H. Levitt, G. Bodenhausen, R.R. Ernst, Progress in NMR Spectroscopy 16 (1983) 163)

A pulse (resonant frequency of the nuclei  $I$  and sometimes also  $S$ ) with angular displacement  $\beta$  and phase  $x$  or  $y$  transforms as (the upper sign and first index refer to the  $x$  phase, the lower sign and second index to the  $y$  phase)

$$I_{x,y} \rightarrow I_{x,y}, \quad (4.42)$$

$$I_{y,x} \rightarrow I_{y,x} \cos \beta \pm I_z \sin \beta, \quad \text{with } \beta = \pi/2 \rightarrow \pm I_z, \quad (4.43)$$

$$I_z \rightarrow I_z \cos \beta \mp I_{y,x} \sin \beta, \quad \text{with } \beta = \pi/2 \rightarrow \mp I_{y,x}, \quad (4.44)$$

$$2I_x S_z \quad \text{with } \beta = \pi/2 \rightarrow -2I_{x,z} S_{y,x}, \quad (4.45)$$

$$2I_y S_z \quad \text{with } \beta = \pi/2 \rightarrow -2I_{z,y} S_{y,x}. \quad (4.46)$$

$I_{x,y}$  and  $S_{x,y}$  stand for single spin coherences and  $I_{x,y}S_{x,y}$  for double spin coherences. The index  $z$  describes the magnetizations. Mixed indices stand for anti-phase coherences. Equations (4.45-4.46) presume that pulses with corresponding phases act simultaneously on the  $I$  and  $S$  spin systems. The pulses acting with the  $x$  phase transform as equ. (4.45) anti-phase coherences in double spin coherences; an anti-phase coherence of the  $I$  nuclei is transferred with the  $y$  phase to an anti-phase coherence of the  $S$  nuclei. In equ. (4.46), the effects in each pulse phase are exchanged.

Under the influence of the scalar coupling ( $\pi JtI_zS_z$ ), we have the following transformations (the upper sign applies to the first index):

$$I_z \rightarrow I_z \quad (4.47)$$

$$2I_xS_y \rightarrow 2I_xS_y \quad (4.48)$$

$$I_{x,y} \rightarrow I_{x,y}\cos\pi Jt \pm 2I_{y,x}S_z\sin\pi Jt \quad \text{when } Jt = 1/2 \rightarrow \pm 2I_{y,x}S_z, \quad (4.49)$$

$$2I_{x,y}S_z \rightarrow 2I_{x,y}S_z\cos\pi Jt \pm I_{y,x}\sin\pi Jt \quad \text{when } Jt = 1/2 \rightarrow \pm I_{y,x}. \quad (4.50)$$

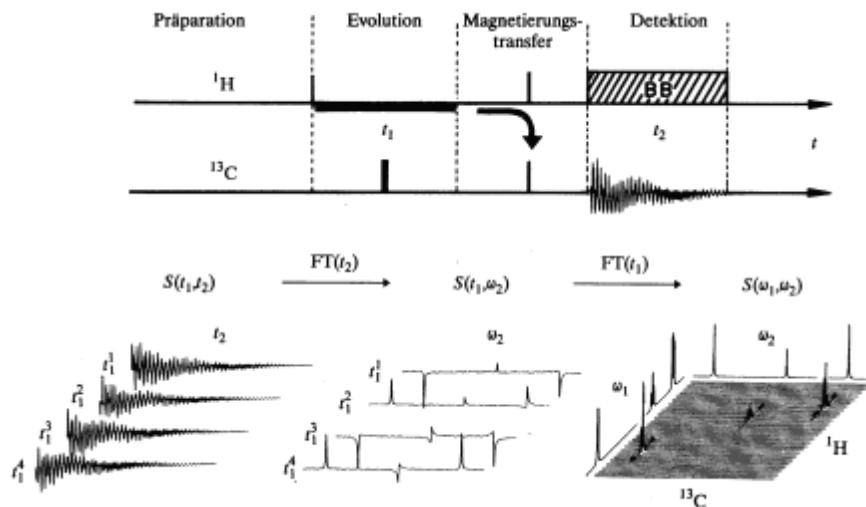
Under the influence of the chemical shift ( $\Omega tI_z$ ), we have the following transformations:

$$I_z \rightarrow I_z \quad (4.51)$$

$$I_{x,y} \rightarrow I_{x,y}\cos \Omega t \pm I_{y,x}\sin\Omega t. \quad (4.52)$$

Two-dimensional (2D) NMR, double resonance, and decoupling will be demonstrated using the example of H,C-COSY (*correlated spectroscopy* or *heteronuclear correlation*, HETCOR) experiment shown in Fig. 4.16. The free induction decay of  $^{13}\text{C}$  nuclei is shown as a function of  $t_2$  and has been Fourier transformed. The  $\omega_2$  scale therefore contains the chemical shift of the  $^{13}\text{C}$  nuclei. Several spectra of this sort are taken for increasing values of  $t_1$  and then Fourier transformed into the second dimension with respect to  $t_1$ . Since the chemical shift developed during the time  $t_1$ , this is shown on the  $\omega_1$  scale. In the 2D spectrum of  $^1\text{H}$ - $^{13}\text{C}$  shift correlation, cross signals only appear in  $^1\text{H}$ - $^{13}\text{C}$  orientations which are directly beside each other. This is an important aid in the ordering of the signals and therefore for structure determination in complicated bonds. Fig 4.16 (Fig. 5 from H. Kessler, M. Gehrke and Ch. Griesinger, *Angew. Chem.* 100 (1988) 507) demonstrates the division of the time scale in preparation (in this experiment, this is only the time of the first  $\pi/2$  pulse), evolution ( $t_1$ ), magnetization transfer ( $2t_1$ ) and detection ( $t_2$ ).

**Fig. 4.16** Principles of the H,C-COSY experiment taken from Kessler et al. Note the changes in intensity of the carbon signals after the first Fourier transformation, in which the evolution of the proton magnetization during  $t_1$  is contained.



In the following description of the spin dynamics of a HETCOR experiment,  $I$  corresponds to the  $^1\text{H}$  and  $S$  to the  $^{13}\text{C}$  spins. Under the influence of the chemical shift of the  $^1\text{H}$  nuclei, the product operator  $I_x$  transforms to  $I_x \cos \Omega_I t + I_y \sin \Omega_I t$  in the time  $t_1$ , see equ. (4.52). In the time  $t_2$ , the chemical shift of the  $^{13}\text{C}$  nuclei acts with  $\Omega_S$  on the  $S$  spins in an analogous way. The influence of the pulses and  $J$  coupling on the spin system will be described in the following representation. Fig. 4.17 assumes that the pulse widths are small compared to  $t_1$ ,  $t_j$  and  $t_2$ .

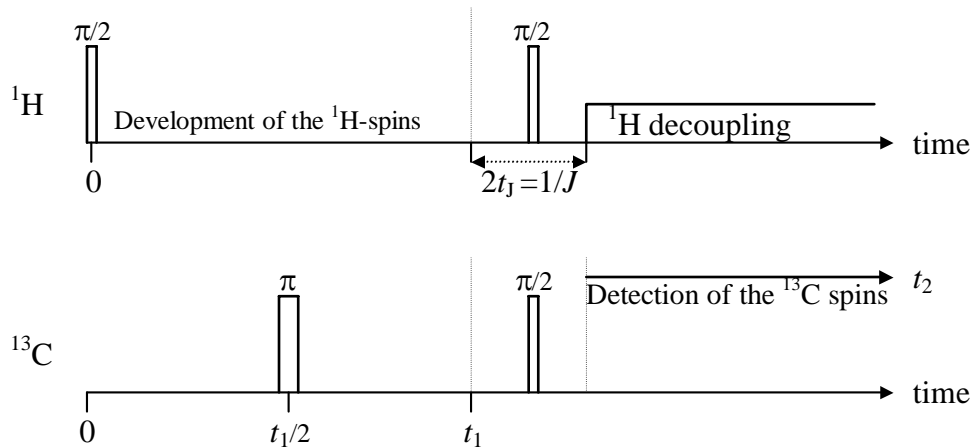


**Fig. 4.17** Pulses and time scales in the H,C-COSY experiment.

The first pulse (preparation pulse) only acts on the  $I$  spins and has an alternating phase:

$$I_z \xrightarrow{\pi/2_{\pm y}(I)} \pm I_x \quad (4.53)$$

This means that the phase of the preparation pulse is rotated by  $180^\circ$  in each of the sequential experiments of signal accumulation. We will show that through alternating phase rectification of the FID in the signal of the  $S$  spin, a few undesirable signal components are removed.

$$\pm I_x \xrightarrow{J_{H-C}} \pm I_x \cos \pi J t \pm 2 I_y S_z \sin \pi J t \quad (4.54)$$

Under the influence of  $J$  coupling, an anti-phase coherence develops according to equ. (4.49). Additionally, the chemical shifts of the  $I$  spins develop. Although they are not seen in the equations, the determination of these shifts is the aim of the experiment.

$$\begin{aligned} I_x \cos \square J t + 2 I_y S_z \sin \square J t &\xrightarrow{\square_x(S)} \\ I_x \cos \square J t + 2 I_y (-S_z) \sin \square J t &= I_x \cos \square J (-t) + 2 I_y S_z \sin \square J (-t). \end{aligned} \quad (4.55)$$

The  $\pi$  pulse acting on the  $S$  spins inverts all occupations of the  $S$  spin at time  $t = t_1/2$ , i.e.  $\alpha$  and  $\beta$  are exchanged and the sign of  $S_z$  is changed. Equation (4.55) makes visible that all the AX interactions of these are removed at time  $t_1$  as a result of "time reversal". Since the  $\pi$  pulse did not, however, act on the  $I$  spins,  $\pm I_x$  is conserved and the development of the chemical shift of the  $I$  nuclei according to equ. (4.52) continues during the entire time period  $t_1$ . As a consequence of the inhomogeneity of the high frequency field, the pulse acts in the middle of the coil as a  $\pi$  pulse. Near the edge of the coil, a small portion of nuclei in a sample which is longer than the coil only experience a  $\pi/2$  pulse. This causes a small transversal magnetization, but is averaged out by phase sensitive rectification with alternating phase.

After the evolution period, the maximal anti-phase coherence develops in the time between  $t_1$  and  $t_1 + t_J$  with  $Jt_J = 1/2$ , see equ. (4.49):

$$\pm I_x \xrightarrow{J_{\text{H-C}}\left(t_J = \frac{1}{2J}\right)} \pm 2I_y S_z. \quad (4.56)$$

The second  $\pi/2$  pulse is input to both the  $^1\text{H}$  and the  $^{13}\text{C}$  nuclei. This causes the transfer of anti-phase coherences according to equ. (4.46) from the  $^1\text{H}$  into the  $^{13}\text{C}$  spin system:

$$\pm 2I_y S_z \xrightarrow{\pi/2_x(I,S)} \mp 2I_z S_y. \quad (4.57)$$

In the subsequent second time interval  $t_J$ , the non-observable anti-phase coherences of the  $^{13}\text{C}$  nuclei become observable transversal magnetization of the  $^{13}\text{C}$  nuclei (see equ. (4.50), in which  $I$  and  $S$  are exchanged):

$$\mp 2I_z S_y \xrightarrow{J_{\text{C-H}}} \pm S_x. \quad (4.58)$$

Afterwards,  $S_x$  develops during  $t_2$  under the sole influence of the external field and the  $^{13}\text{C}$ - $^{13}\text{C}$ -interactions, since through the strong input of the  $^1\text{H}$  frequency, their spins are constantly flipping and thus have no influence on the  $^{13}\text{C}$  spins on average. The detection takes place with alternating phase. Besides the part of the signal from the inhomogeneity of the  $\pi$  pulse, also the part  $S_z$  from the second  $\pi/2$  pulse which became transversal magnetization (not considered above) is removed.

## 4.8 NMR Imaging

MR (magnetic resonance) tomography, also known as magnetic resonance imaging (MRI), is an imaging method based on NMR. Optional equipment for MR scanner (1 million € higher price) allows a spatially resolved spectroscopy. Applications in medicine have become so important that the principle of tomography will be considered here without spectroscopy.

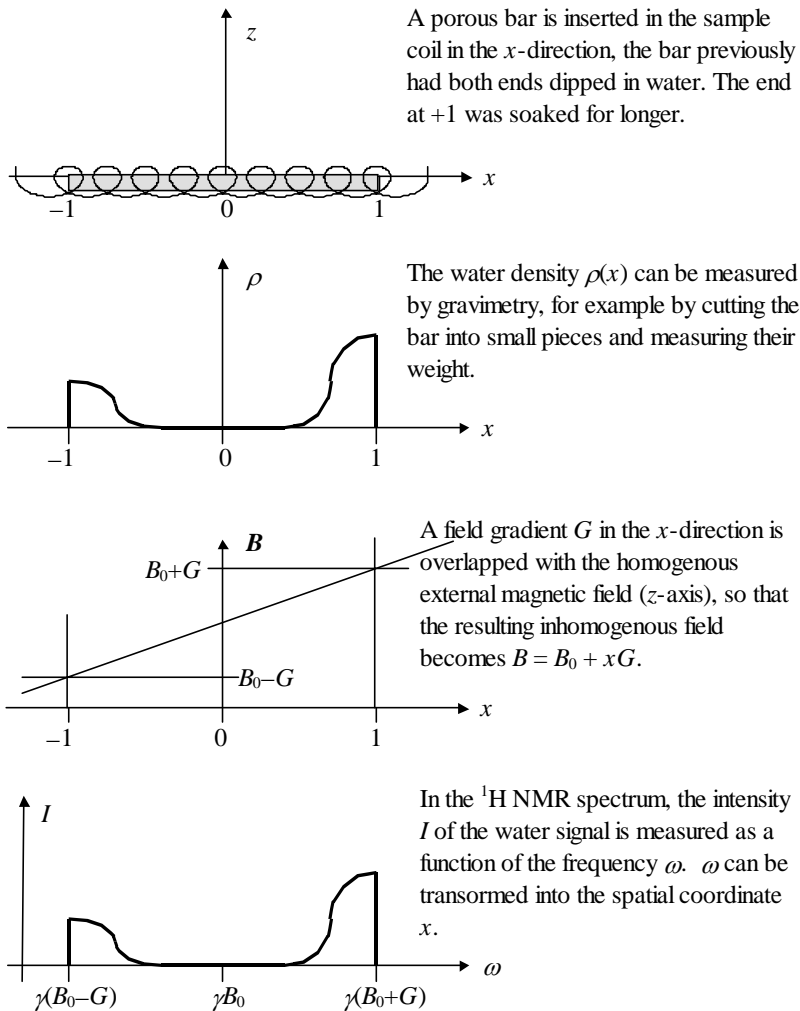


**Fig. 4.18** Principle of one-dimensional tomography.

Three-dimensional tomography requires gradient coils, which create three-dimensional orthogonal gradients and can be quickly switched on and off (within 1 ms). In the presence of a gradient in the  $z$ -direction, a selective  $\pi/2$  pulse is applied which, in a selected plane perpendicular to the  $z$ -direction, flips the magnetization  $M$  per mol from the  $z$ -direction into the  $x$ - $y$ -plane. We then get as a signal in the time domain:

$$S(t) = \iint dx dy M \rho(x, y) \exp(i\mathbf{r}\mathbf{k}) f(T_1, T_2), \quad (4.59)$$

$\rho(x, y)$  is the proton density in mols per unit volume,  $k(t) = \gamma \int \mathbf{G}(t) dt$  with  $G(t)$  is the field gradient vector, and  $f(T_1, T_2)$  are exponential functions of the relaxation times. The image is sampled in successive experiments in the  $k$ -plane with a fixed  $x$  but a varied  $y$  gradient, in which the  $y$  gradient is only present between the two HF pulses of the Hahn echo pulse sequence. A double Fourier transformation of  $S(t)$  with respect to  $k_x$  and  $k_y$  results in the density function for a selected  $z$  in the  $x$ - $y$ -plane.

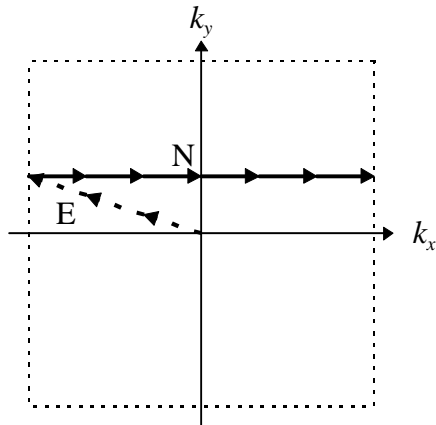


**Fig. 4.19** The sampling of the  $k$ -plane.  $E$  refers to the development path and  $N$  to the detection path.

In Fig. 4.19,  $E$  describes the development, in which  $G_x$  was chosen to be negative and  $G_y$  positive.  $N$  is the detection path, in which  $G_y = 0$  and  $G_x$  is positive. rf pulses, gradient pulses and the time signal are shown in Fig. 4.20.

The previous discussion ignores relaxation during the development and detection period. The signal is proportional to the density of nuclei, e.g.  $^1\text{H}/\text{cm}^3$ . Relaxation effects cause a reduction in signal intensity and can be used to give an additional contrast. At 0,15 Tesla, in a  $^1\text{H}$  NMR signal, a healthy liver has a longitudinal relaxation time of  $T_1 \approx 250$  ms, but a liver metastasis has one of  $T_1 \approx 750$  ms. To blend out the signal of the healthy liver, the pulse sequence could be preceded by a  $\pi$  pulse with a delay of  $(250 \cdot \ln 2)$  ms, see chapter 4.3. Also for various transversal relaxation times, such as in healthy brain:  $T_2 \approx 100$  ms, brain tumor  $T_2 \approx 200$  ms, contrasts can be changed by varying the distance between the pulses in the Hahn echo.

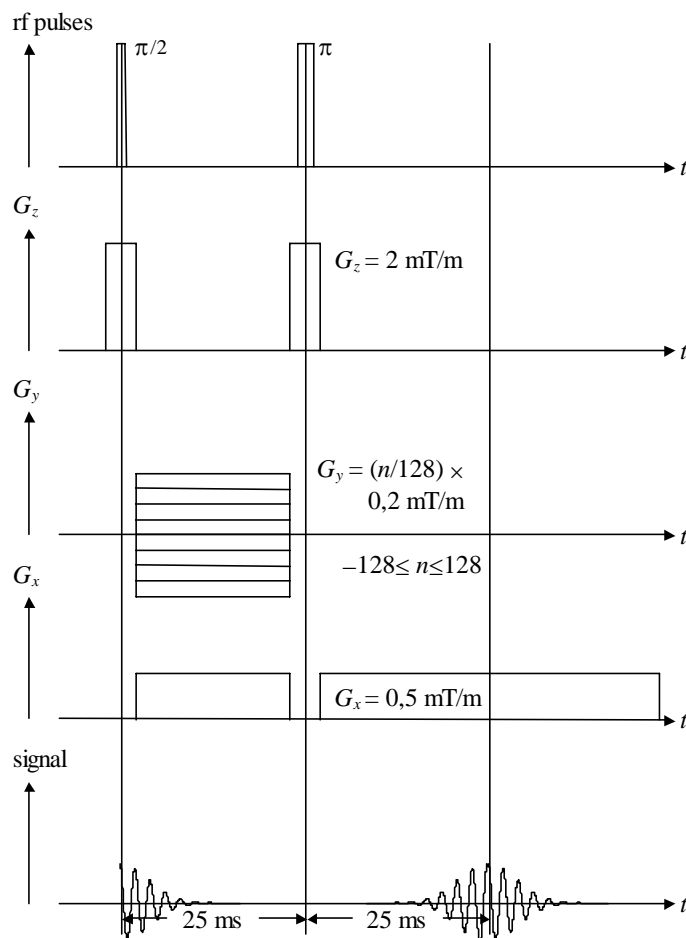


**Fig. 4.20** Pulse and gradient program for MRI. This example is good for lectures, but rarely applied in practice.

## 4.9 Literature

- Abragam A.: The Principle of Nuclear Magnetism, Oxford University Press, 1978  
 Bigler P.: NMR Spectroscopy: Processing Strategies, Wiley-VCH Weinheim 1997  
 Braun S., Kalinowski H.-O., Berger S.: 150 and More Basic NMR Experiments, Wiley-VCH Weinheim 1998  
 Breitmaier E., Voelter W.: Carbon-13 NMR Spectroscopy, VHC Verlagsgesellschaft Weinheim 1987  
 Callaghan: Principles of NMR microscopy, Clarendon Press, 1991  
 Canet, D.: NMR-Konzepte und Methoden, Springer-Verlag, 1994, ISBN 3-540-58204-5  
 Croasmun, W.R. and R.M.K. Carlson: Two-Dimensional NMR Spectroscopy, VCH, 1994, ISBN 1-560981-664-3  
 Duer M. (ed.): Solid-state NMR, Blackwell Science, 2002, 0-632-05351-8  
 Dybowski C., Lichter R.L.: NMR Spectroscopy Techniques, Marcel Dekker, Inc., New York, 1987  
 Ernst R.R., Bodenhausen G. and Wokaun A.: Principles of NMR in One and Two Dimensions, Oxford University Press, 1986  
 Freemann R.: A Handbook of Nuclear Magnetic Resonance Spectroscopy, Longman, 1987  
 Friebolin H.: Basic One- and Two-Dimensional NMR-Spectroscopie, Wiley-VCH Weinheim, 1993  
 Fukushima E. Roeder S.B.W.: Experimental Pulse NMR, Addison-Wesley Publishing Company, Inc. 1981  
 Fyfe C.A.: Solid State NMR for Chemists, C.F.C. Press, 1983  
 Gerstein B.C., Dybowski C.R.: Transit Techniques in NMR of Solids, Academic Orlando, 1985  
 Günther H.: NMR Spektroskopie (<sup>1</sup>H NMR), Georg Thieme Verlag Stuttgart, 1983  
 Haeberlen U.: High Resolution NMR in Solids, Academic Press, 1976  
 Harris R.K.: Nuclear Magnetic Resonance Spectroscopy, Longman, 1986  
 Hennel, J.W., Klinowski, J.: Fundamentals of NMR, Longman, Essex 1993, 288 S., ISBN 0 582 06703 0  
 Hesse M., Meier H., Zeeh B.: Spektroskopische Methoden in der organischen Chemie, Georg Thieme Verlag Stuttgart, 1987  
 Kitamaru R.: Nuclear Magnetic Resonance, Principles and Theory, Elsevier, 1990  
 Kleinpeter E., Borsdorf R.: <sup>13</sup>C-NMR in der organischen Chemie, Akademie Verlag, 1981  
 Mehring M.: Principles of High Resolution NMR in Solids, Springer-Verlag, 1983  
 Michel D.: Grundlagen und Methoden der kernmagnetischen Resonanz, Akademieverlag, 1982  
 Poole C.P. and Forach H.A.: Theory of Magnetic Resonance, Wiley 1987  
 Rahman A.: One and Two Dimensional NMR Spectroscopy, Elsevier, 1989  
 Sanders J.K.M. and Hunter B.K.: Modern NMR Spectroscopy, Oxford University Press, 1987  
 Schraml J., Bellama J.M.: Two-Dimensional NMR Spectroscopy, John Wiley, 1988  
 Slichter C.P.: Principles of Magnetic Resonance, Springer-Verlag, 1989  
 Weber U., Thiele H., Hägele G.: NMR-Spectroscopy: Modern Spectral Analysis, Wiley-VCH Weinheim

### MRI in Medicine:

- M.T. Vlaardingerbroek, J.A. den Boer: Magnetic Resonance Imaging, Springer 2002 or M.T. Vlaardingerbroek, J.A. den Boer: Magnetresonanztomographie, Springer 2004, ISBN 3 540 20028 2  
 R.H. Hashemi, W.G. Bradley: MRI the Basics; Williams & Wilkins 1997  
 C.Westbrook, C.Kaut: MRI in Practice; Blackwell Science 1998  
 L.Dilcher, M.Venator, S.Dilcher: Kleines Handbuch der Kernspintomographie; Edwin Ferger Verlag 1997; ISBN 3-931219-02-X  
 M. NessAiver: All you really need to know About MRI Physics; Simply Physics, Baltimore 1997, ISMN 0-9660982-0-X